공학석사학위논문

Development of tungsten sintering technology for fusion applications

핵융합로용 텅스텐 대면소재의 소결 기술 개발

2017년 2월

서울대학교 대학원

재료공학부

성 현 민

ABSTRACT

In this study, sintering conditions to obtain high-density sintered tungsten materials with thermal stability were studied utilizing spark plasma sintering method (SPS). Sintering factors such as sintering powder condition, temperature, time, pressure and process were independently controlled to figure out their effects. The microstructure and properties of samples sintered under each controlled condition were feedbacked to obtain optimized sintering conditions. The thermal stabilities of tungsten samples were evaluated by high heat flux (HHF) test. The microstructures of sintered samples after HFF test were compared with those of the Plansee ITER grade tungsten samples after HHF test. It was revealed that the high-density sintered tungsten samples fabricated by SPS possess better microstructural stability and mechanical property than Plansee ITER grade tungsten samples under elevated temperature conditions. Additionally, improvement of mechanical properties of tungsten materials were also investigated.

Keywords: Plasma-facing materials, Tungsten, Spark plasma sintering, High heat flux test, Thermal stability, Electron backscatter diffraction and Mechanical property.

Student Number : 2015-20830

Contents

LIST OF FIGURES

LIST OF TABLE

1. Introduction

With the limited amount of fossil fuels and worries on greenhouse effect, human being is searching for a new safe and clean next-generation power source. As one of the most promising next-level power generation method, fusion power generation is spotlighted worldwide.

Korea (Republic of Korea) is a member of an international fusion reactor project, called ITER (International Thermonuclear Experimental Reactor) cooperate with many countries such as United States of America, China, Japan, India, France, European Union and Russia (Figure 1). ITER is an in-construction reactor in southern France, planned to be completed by 2025. As a member of ITER project, Korea is in charge of supplying various parts of reactor (procurement parts) including superconductor, tritium storage system and in-vessel components etc. Therefore, researches on ITER project procurement parts are active in Korea. However there are minor researches on non-procurement parts such as plasma-facing materials (PFMs). The PFMs are the materials consisting plasma-facing components (PFCs) such as first wall and divertor. (Figure 2) PFCs are the parts determine the stability of the structure of fusion reactor and strongly affect the stability of plasma. For the development of Korean fusion reactor such as Korea Superconducting Tokamak Advanced Research (KSTAR) (Figure 3) and Korea DEMOnstration power station (KDEMO), Korean researches on plasma-facing materials are

essential.

As PFCs are exposed to the harsh plasma condition such as neutron or ion irradiation and high heat flux condition (Figure 4), applicable PFMs are limited [1]. In the early researches on the PFMs, carbon materials such as graphite were investigated. Properties of carbon materials such as high melting point, light weight, good thermal conductivity and low central radiation loss were suitable as PFMs. However, its high erosion rate at operating temperature of the fusion reactor, degraded thermal conductivity by neutron damage and high tritium retention limited the application of carbon materials to the PFCs [2-4]. Tungsten is one of the most promising candidate material as PFM which can replace carbon materials due to its physical properties such as high melting point, high thermal conductivity, low tritium retention, low sputtering rate and low erosion rate [5-11].

In this study, sintering conditions to fabricate high-density tungsten were successfully obtained utilizing spark plasma sintering and their thermal stabilities were evaluated by high heat flux (HHF) test. Due to high melting point of tungsten, tungsten is normally produced by sintering process. Sintering process is a process consolidating powders into bulk by diffusion at high temperature lower than the melting point of the material. In the sintering process, various factors such as sintering temperature, time, heating rate and powder conditions affect final sintered products. It is necessary to optimize the sintering condition to produce high-density sintered materials. Spark plasma

sintering method (SPS) is a noble sintering method applying electric current directly to the mold containing powder for the use of electric current effects. Even though the detailed effects of electric current are not elucidated, it is well known that the sintering process could be accelerated by SPS, enabling to achieve high-density sintered materials at a relatively low sintering temperature in short time comparing to the conventional sintering methods [12,13]. Therefore, spark plasma sintering method was utilized in this study and the optimization of sintering conditions by controlling sintering factors was performed to obtain high-density sintered tungsten. To verify the fusion applicability of fabricated tungsten samples by evaluate their thermal stability, HHF test was conducted. For the comparison between fabricated high-density tungsten samples and commercial fusion grade tungsten, Plansee ITER grade tungsten samples were also investigated. Effects of thermo-mechanical process on tungsten materials were also investigated for the improvement of the mechanical property of the sintered tungsten samples. The microstructure of samples were observed using optical microscope (OM), field emission scanning electron microscope (FE-SEM) with electron backscatter diffraction (EBSD), energy dispersive x-ray spectroscopy (EDS) and Auger electron spectroscopy (AES). In addition, Vickers hardness test and Archimedes method were used to measure properties of samples such as hardness values and relative densities.

Figure 1. Schematic diagram of International Thermonuclear Experimental Reactor [14].

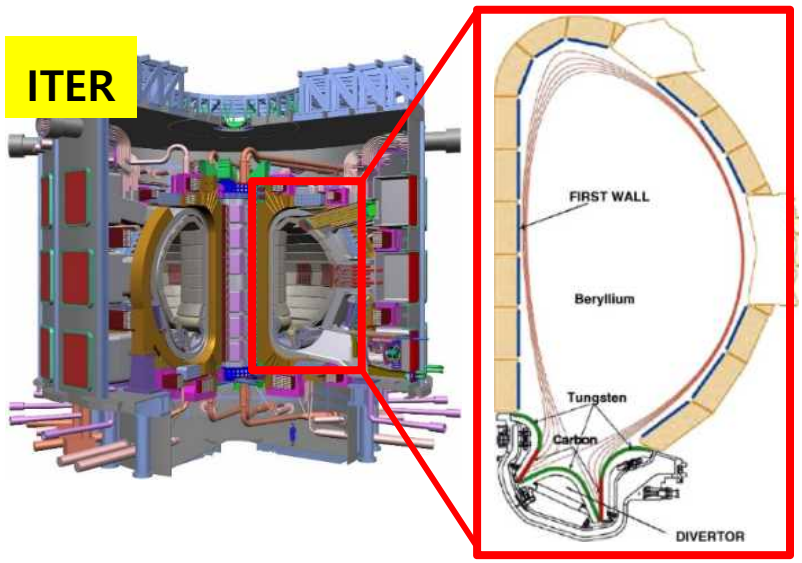

Figure 2. Plasma facing components in fusion reactor [15].

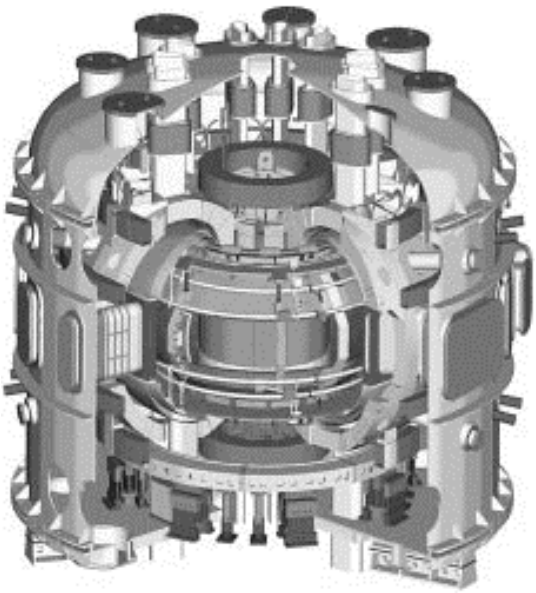

Figure 3. Configuration of tokamak of Korea Superconducting Tokamak Advanced Research (KSTAR) [16].

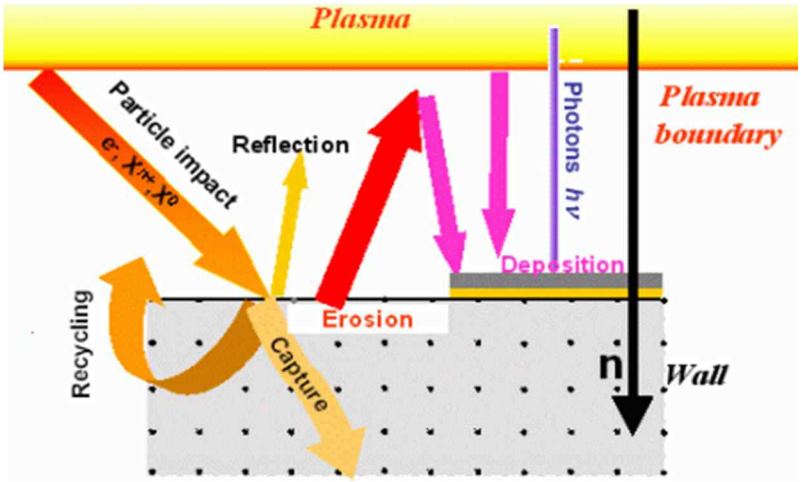

Figure 4. Interactions between plasma and plasma-facing materials [17].

2. Theoretical Backgrounds

2.1 Tungsten as Plasma Facing Material

2.1.1 Fusion Reaction and Tokamak

The nuclear fusion reaction is a fusion reaction between deuterium (D) and tritium (T) atoms at high temperature producing one helium atom, one neutron (n^0) and massive heat energy (Figure 5). More specifically, the fusion reaction of D-T nuclei generates one He atom and one n^0, wherein the mass of the produced He and n^0 is smaller than the sum of the D and T mass before the reaction. These mass loss is converted into energy by Einstein's mass-energy conversion formula ($E=mc^2$) and released as massive amount of heat.

An atom is composed of nucleus and electrons, and the atomic nucleus is surrounded by electron cloud. In this normal state, atoms cannot take fusion reaction as it is hard to reach other atom's nucleus. At high temperatures above 1,000,000 K, the nucleus and electrons are separated from each other forming an ion-cloud-like state, which is called a plasma (Figure 6). Even though the atomic nucleus and the electrons are separated forming plasma at high temperatures above 1,000,000 K, the fusion reaction cannot occur due to the repulsive force between each nucleus. In order to overcome this repulsion and to fuse the D-T nuclei, it is necessary to overcome the repulsion by increasing the kinetic energy of the nucleus. Since the temperature of a material is the same as the kinetic energy of an atomic nucleus, increasing temperature of the plasma

will make fusion reaction to occur overcoming the repulsion between nuclei in the plasma. This D-T fusion reaction is the same reaction happens in the Sun. In the Sun, the starting temperature of the fusion reaction is about 15,000,000K, but due to the difference in reaction pressure caused by the difference in the gravitational force between the Earth and the Sun, it is known that the temperature above 100,000,000K is required to initiate the D-T fusion reaction on Earth.

Fusion reaction temperature is the reason why people uses hydrogen isotope in fusion reaction. Fusion reaction could be done with many other elements, however with increasing atomic number, the repulsive force between atomic nuclei increases which increases fusion initiation temperature. As hydrogen is the most light-weight atom (Z=1), the starting temperature of the fusion reaction is relatively lower than any other elements.

In order to generate electricity using heat from the fusion reaction, it is necessary to confine the high temperature plasma at a certain place extracting heat continuously. Since no solid material can directly contact and bear the high temperature plasma, a torus chamber using magnetic field has been designed to confine the plasma, avoiding direct contact with the material.

As mentioned above, the plasma could be controlled by magnetic fields, as the nucleus and electrons of the atom are separated from each other forming an ion-cloud-like state, the plasma. A device for confining and controlling the plasma by magnetic field is called tokamak (TOroidamaya KAmera

MAgnitnaya Katushka) (Figure 7). The tokamak is a device designed in Russia, and its meaning is a toroid-shaped vessel (TOroidalnaya KAmera) and a magnetic coil (MAgnitnaya Katushka). The control of the plasma using the tokamak is performed by using a magnetic field in a toroidal direction formed by superconductor coil wound in a torus shape and a poloidal magnetic field formed by current flowing on the plasma. The combination of these two magnetic fields creates a spirally twisted magnetic field around the torus and confines the high temperature plasma into the torus. Pinch effect is known to happen when current is flowing on the gas which shrinks the gas by attraction force between parallel currents flowing in the same direction. This effect shrinks the plasma so that the plasma cannot not directly contact the material consisting the fusion reactor. Most of the fusion reactors under investigation worldwide are adopting the form of tokamak. In addition to the control of the fusion plasma using the magnetic field, other plasma control methods such as inertial confinement fusion are being studied. However, due to the persistence of the reaction and the stability of plasma, tokamak is the most promising form of fusion reactor. ITER, DEMO, and KSTAR, which is a Korean test reactor, all adopt the tokamak form.

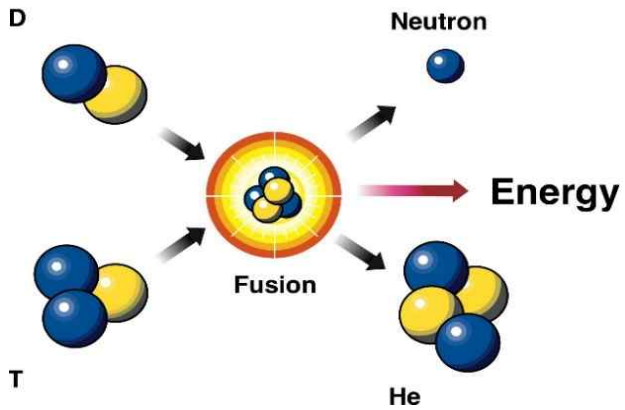

Figure 5. Fusion reaction of Deuterium and Tritium [18].

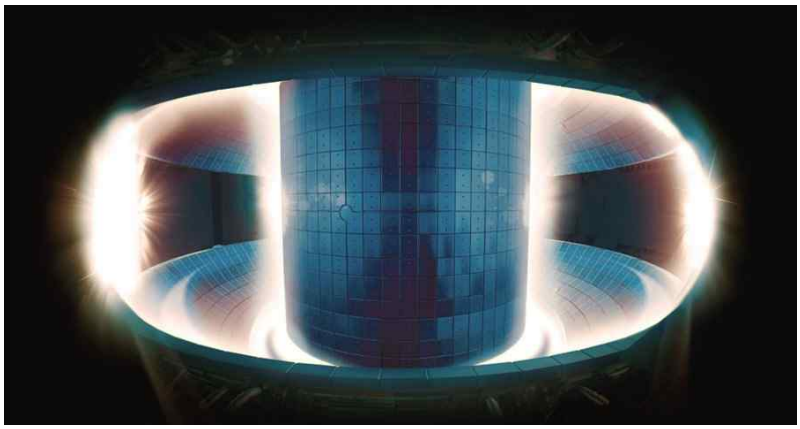

Figure 6. Plasma in Korea Superconducting Tokamak Advanced Research (KSTAR) [14].

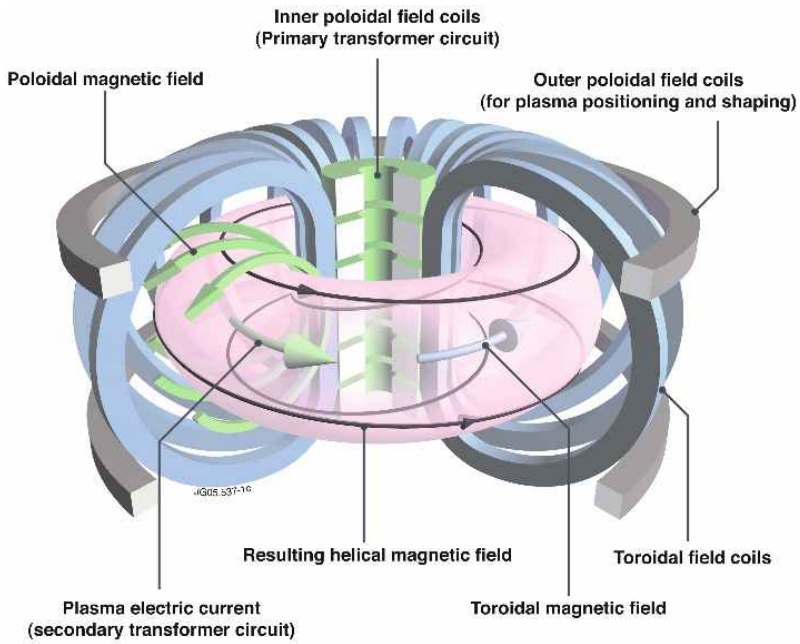

Figure 7. Plasma confinement using tokamak [19].

2.1.2 Plasma Facing Material

The plasma-facing components (PFCs) are the plasma-facing part closest to the plasma inside the tokamak (Figure 2). PFCs are parts locates inside the tokamak such as first wall and divertor. These PFCs are important components as they determine the safety of the fusion reactor and the stability of the fusion reaction. The materials used to construct PFCs are called plasma-facing materials (PFMs). The PFMs are the utmost important factor as they determine the performance of the PFCs [5-11].

In the first wall, heat and particles from the fusion reaction of the plasma are irradiated. A water cooling tube is located behind the first wall, and the absorbed thermal energy which was generated by the fusion reaction of the plasma is used to boil water rotating the turbine. Divertor plays a role of removing heat and ashes from fusion reaction. It is generally located at the bottom of the fusion reactor (Figure 8), and it is known that divertor parts are irradiated by higher heat flux and particle than the first wall. In other words, the operating window of the first wall and the divertor is different [1] and this is why different materials were applied in the first wall (Be) and the diverter (W) in the ITER.

In the fusion reactor, interaction between plasma and PFMs results in damage on PFCs and affects the stability of plasma [20-26]. The damages on PFCs come from the irradiated particles such as n^0 or H/He/W ions and the thermal loads. By the irradiated particles, PFCs surface morphology and

microstructures could be degraded resulting formation of defects such as nano-fuzz, pores and blisters (Figure 9 (a) and (b)). By thermal load, surface cracking or melting could be take place (Figure 9 (c) and (d)). Continuity of fusion reaction is determined by applying low T retention materials, which are less-tritium absorbing materials. Some materials highly absorb T in fusion reactor causing nuclear contamination of PFMs and loss of fuels to react (D and T) [27]. Controlling of the impurity contents in the plasma which are sputtered or melted out from the PFCs is important for the stable fusion reaction in plasma. When impurities are ejected to the plasma, heat energy of plasma is absorbed by impurity to heat up impurity particle lowering the temperature of plasma. This could shut down the plasma or significantly lowering the power efficiency. Divertor parts play important role of removing impurities in the fusion reactor. Also, by the Bremsstrahlung (German word meaning “deceleration radiation”), the amount of energy loss caused by impurity is proportional to the square of its atomic number ($\propto Z^2$). Therefore, materials with low Z or low sputtering rate is required. Low Z of the beryllium is one of main reasons chosen as the first wall material in ITER.

To secure the safety of fusion reactor and fusion reaction, PFMs with high melting point, low tritium retention, high thermal conductivity and low sputtering and erosion rate are required.

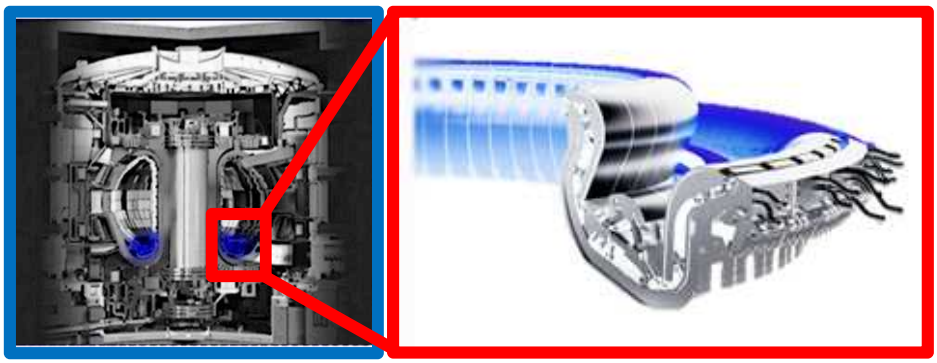

Figure 8. Position of divertor cassettes in fusion reactor [14].

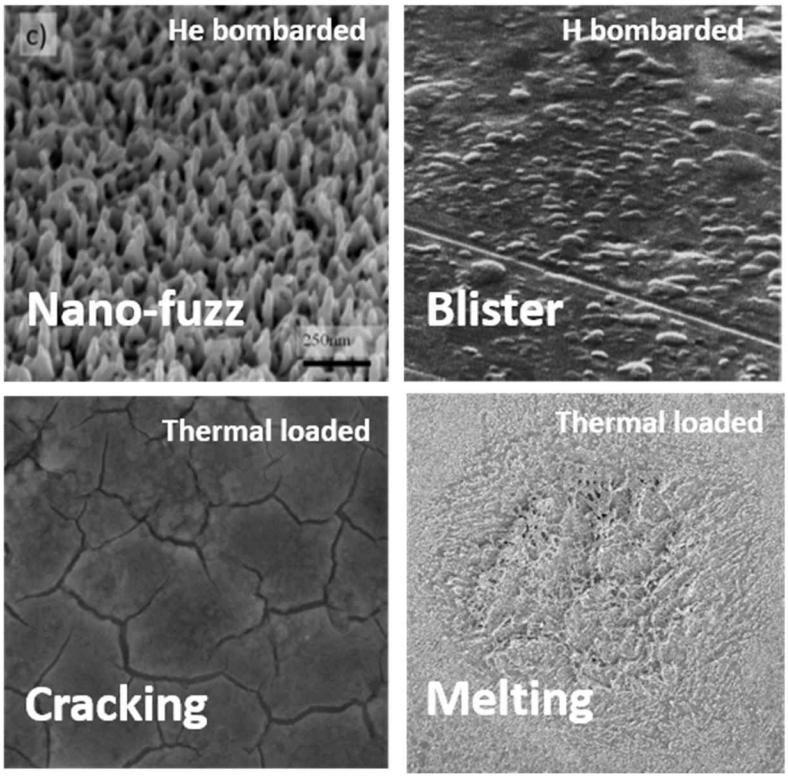

Figure 9. Damages caused by plasma in plasma-facing materials [22,26,28].

2.1.3 Tungsten as Plasma Facing Material

As mentioned above, PFMs with high melting point, low tritium retention, high thermal conductivity and low sputtering and erosion rate are required. In the early stages of fusion researches, carbon materials such as graphite were under consideration as PFM [2-4]. Carbon materials possess strong points in its high melting point, light weight, good thermal conductivity low central radiation loss and low-Z. However its high erosion rate at high temperature, high T retention and loss of thermal conductivity after n^0 irradiation limits its applications. As an alternative, application of tungsten materials as PFM is being considered [5-11]. Tungsten has highest melting point (~3700K) and lowest vapor pressure ($1.3x10^{-7}$Pa at T_m) among pure metals with 6th highest thermal conductivity (174W/m · K at R.T). Also, it possesses high threshold energy resisting sputtering, low tritium retention, low erosion rate and high thermal stability. Due to such excellent properties as PFM, tungsten is currently accepted as divertor material in ITER and under consideration to be applied for first wall and divertor in DEMO.

For the ITER, tungsten specification requirements are as follows: 1. chemical composition minimum is 99.94%, 2. Density minimum is 19.0/cm^3 (relative density of 98.7%), 3. Stress relieved condition (not recrystallized), 4. Average grain size should not exceed 90μm, 5. Hardness have to exceed 410HV30. However, these specifications are just following ASTM B760 (Tungsten Plate, Sheet and Foil) established without consideration of fusion

plasma condition. Additionally, it was reported that the performance of tungsten materials under plasma condition is affected by its production history, grain developed direction and grain orientation. The discussions of standard specifications of tungsten materials for fusion application are still on-going.

2.2 Spark Plasma Sintering

In this study, a noble sintering method called spark plasma sintering method (SPS) is utilized (Figure 10). SPS is a sintering method applying direct electric current to the graphite mold containing powder materials inside. As SPS uses direct electric current to the mold as a heating source, the heating rate and the cooling rate are much faster compare to the conventional sintering methods. Also the sintering efficiency of SPS is excellent comparing to the other general sintering method. In general sintering method such as pressurized or pressureless sintering, it is difficult to obtain a high-density materials even at a high temperature and in a long sintering time. However, it is well-known that a high-density sintered materials could be obtained in a remarkably short time and at low temperature with SPS. Figure 11 compares the microstructure of pressureless sintered and spark plasma sintered tungsten samples. In the spark plasma sintered sample, it can be seen that the size of pores are much smaller than pressureless sintered sample showing better sinter-ability of SPS, at the short sintering time and low sintering temperature comparing to the pressureless sintering method.

Electric current has been reported to affect materials property and microstructure by distinctive electric current effects. Starting with Machlin report in 1959 that the materials ductility, flow stress and yield stress could be affected by electric current [29], numerous researches have supported the existence of electric current effects. Though the detailed mechanism has not

been elucidated, various theories such as electron wind effect [30,31], electrostatic field effect [32,33] and Joule heating effect [34,35] has been suggested. From the recent studies using electro-heat treatment, it is reported that the annealing of Al alloy [36] and dissolution in Mg alloy could be accelerated by electric current. Also, reduce of splat boundaries in air plasma sprayed tungsten using electric current treatment was also reported in 2016 [5]. These results suggest that the electric current could accelerate atomic diffusion in metallic materials including tungsten. Therefore, the SPS was selected to study fabrication of high-density sintered tungsten materials.

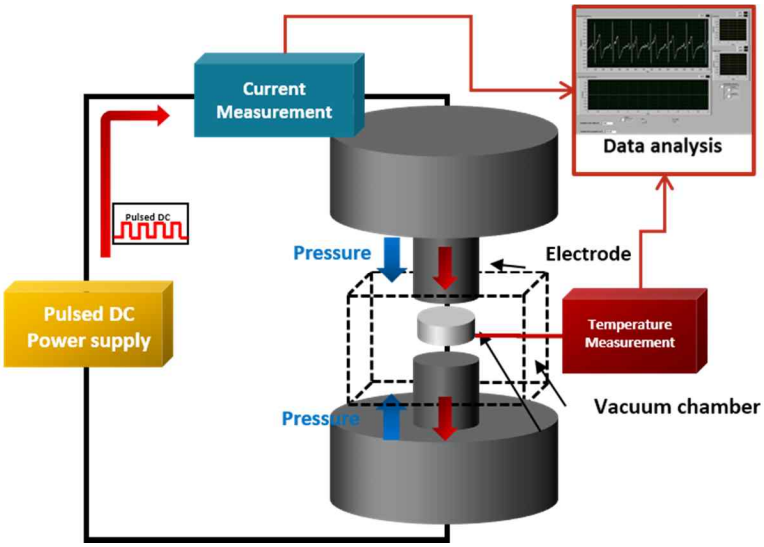

Figure 10. Schematic diagram of spark plasma sintering.

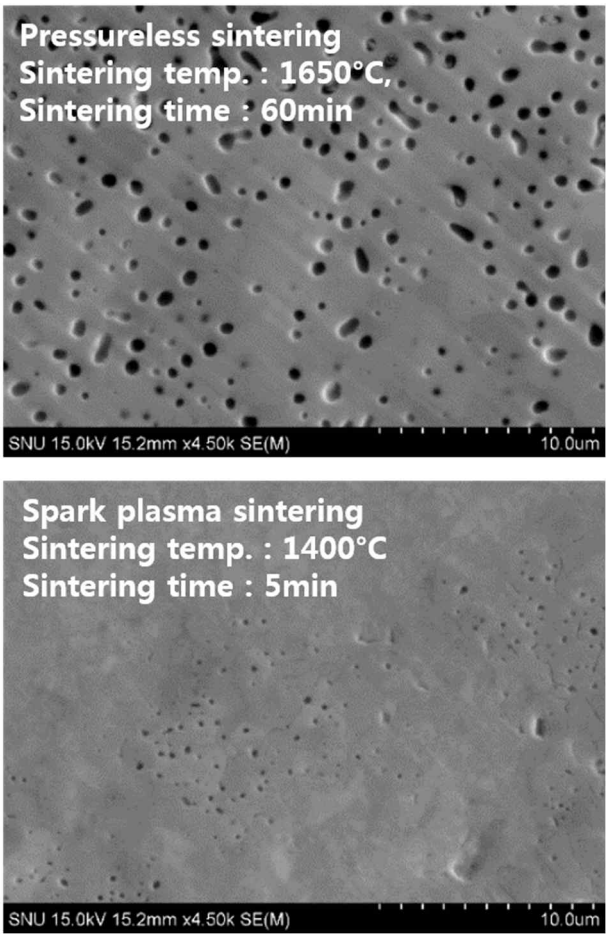

Figure 11. Microstructure of the pressureless sintered sample and the spark plasma sintered sample.

3. Experimental

3.1 Powder Preparations

The tungsten powder (>99.9% pure tungsten) used in the experiment is manufactured by TaeguTec. The powder used in this study was WP04 with an average particle size of 0.5μm, WP23 with an average particle size of 2.4μm and WP45 with an average particle size of 4.8μm. Through microstructures observations of sintered materials, small average particle size was found to be the most favorable for sintering. Therefore, most of sintering done in this study used WP4 powder with average particle size of 0.5μm.

From the experimental results, it was confirmed that the usage of as-received power made some high-oxygen content area in the sintered sample. To solve this problem, WP04 was reduced in a hydrogen atmosphere. The H_2 reduction treatment temperature is determined based on the thermodynamic calculations using FactSage (Figure 12). In this study, there are two kinds of reduction treatment conditions.

The H_2 reduction heat-treatment conditions are like below:

Heat treatment of 24 hours under 100% H_2 atmosphere at 900°C

Heat treatment of an hour under 100% H_2 atmosphere at 1100°C

The morphology of as-received and reduce powders are shown in Figure 13.

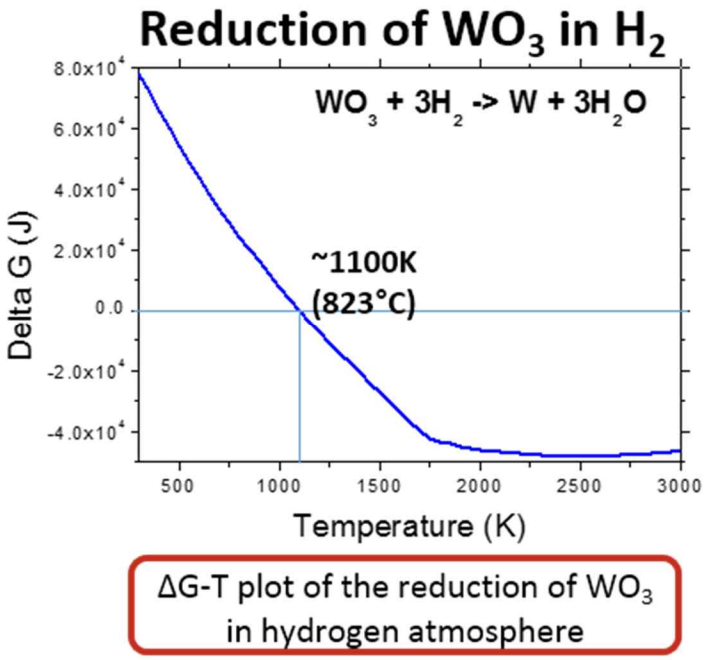

Figure 12. Thermodynamic calculation on reduction of WO_3 in 100% H_2 atmosphere using FactSage.

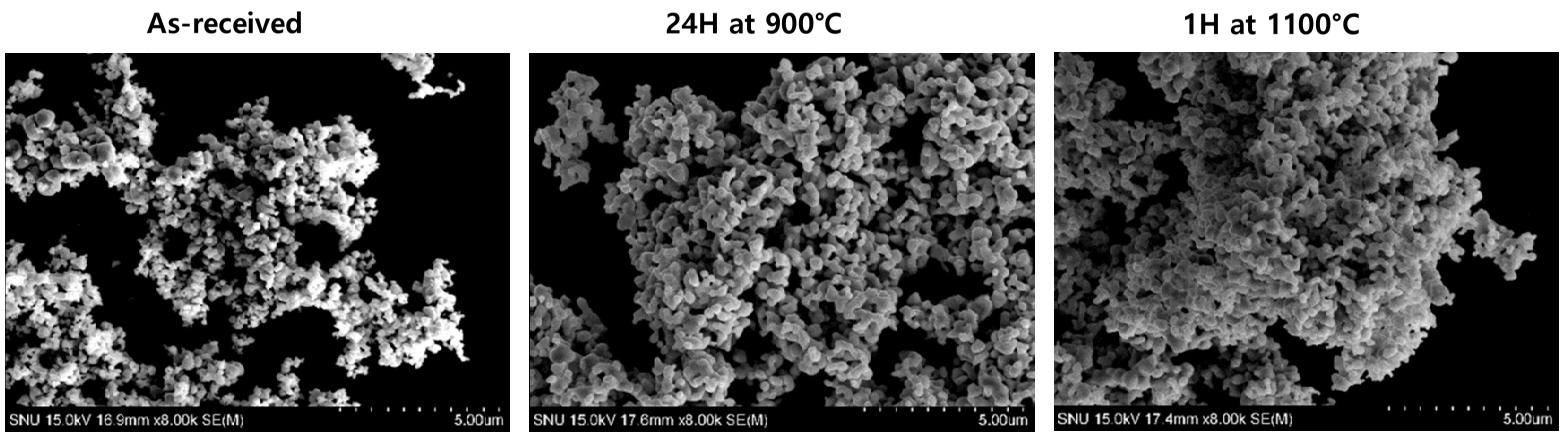

Figure 13. Morphologies of as-received and reduced powders.

3.2 Spark Plasma Sintering

In this study, sintering was carried out using SPS. The SPS equipment used in this study is domestic equipment manufactured by Weltech Co., Ltd (Figure 14). Graphite mold (inner diameter of 10.5mm, an outer diameter of 20mm and the height of 40mm) and graphite electrode (diameter of 10mm and height of 30mm) were used for the sintering. In order to prevent carbon contaminations of samples by graphite mold, a 0.5mm thick carbon sheet was wrapped inside of the graphite mold, to avoid direct contact between powders and graphite mold. Graphite molds were manufactured by domestic company named Dongbang Carbon Co., Ltd. For each sintering, 5 grams of tungsten powder were used. The sintering temperature was measured using a 2-channel pyrometer.

The purpose of this study is to develop a tungsten sintering technology for fusion applications. Commercial ITER grade tungsten materials were produced by general sintering at temperatures above 2200℃ achieving nearly relative density of 80% and then deformed by thermo-mechanical process such as rolling or forging to get a highly-densified product (Figure 15). With SPS, it is able to achieve high-density sintered samples without thermo-mechanical process at lower temperatures and shorter time than known sintering conditions for tungsten. Therefore, the optimization of sintering conditions using SPS for the high-density sintered tungsten was performed in this study.

Controllable sintering factors include sintering temperature, time, sintering process, powder particle size, powder reduction treatment, and heating rate. In this study, we searched for the optimized conditions to fabricate high-density sintered tungsten samples by controlling those factors independently. The microstructure observations and property measurements were done for all of the sintered samples, and the analyzed results were feedbacked for the optimization of the sintering condition (Figure 16).

1. Control of powder particle size

   Powders having an average particle size of 4.8μm, 2.4μm and 0.5μm were respectively sintered using single step sintering process for 5 minutes at 1500°C with heating rate of 100°C/min and under a pressure of 25 MPa.

2. Control of sintering temperature

   Powder having an average particle size of 0.5μm was sintered using single step sintering process for 10 minutes at 1300°C, 1400°C, 1500°C, 1600°C respectively with heating rate of 100°C/min and under a pressure of 35 MPa.

3. Control of sintering time

   Powder having an average particle size of 0.5μm was sintered using single step sintering process for 5 and 10 minutes respectively at 1600°C with heating rate of 100°C/min and under a pressure of 35 MPa.

4. Control of sintering process

   Powder having an average particle size of 0.5μm was sintered using single step and two step sintering (TSS) respectively. Sintering was done for 5 minutes of sintering time under a pressure of 35 MPa with heating rate of 100°C/min. In the single step sintering, sintering temperature was 1600°C and for the TSS, the first sintering temperature (T_1) was 1600°C and second sintering temperature (T_2) was 1300°C.

5. Control of heating rate

   Powder having an average particle size of 0.5μm was sintered using TSS process for 5 minutes at T_1 1600°C and T_2 1300°C with heating rate of 50°C/min and 100°C/min respectively under a pressure of 60 MPa.

6. Control of powder condition

   The as-received powder and reduced powder having an average particle size of 0.5μm were sintered using TSS process for 10 minutes at T_1 1700°C and T_2 1400°C with heating rate of 100°C/min under a pressure of 60 MPa.

Figure 14. Spark plasma sintering device.

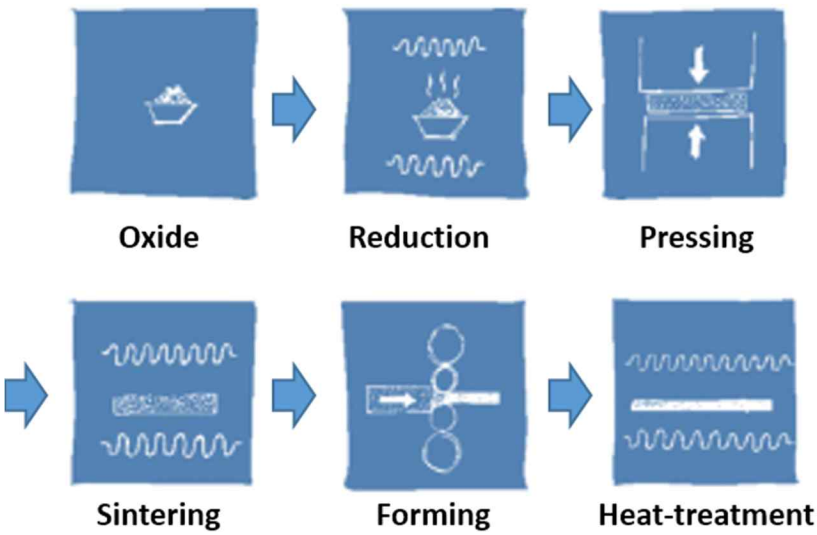

Figure 15. Manufacturing process of tungsten materials [37].

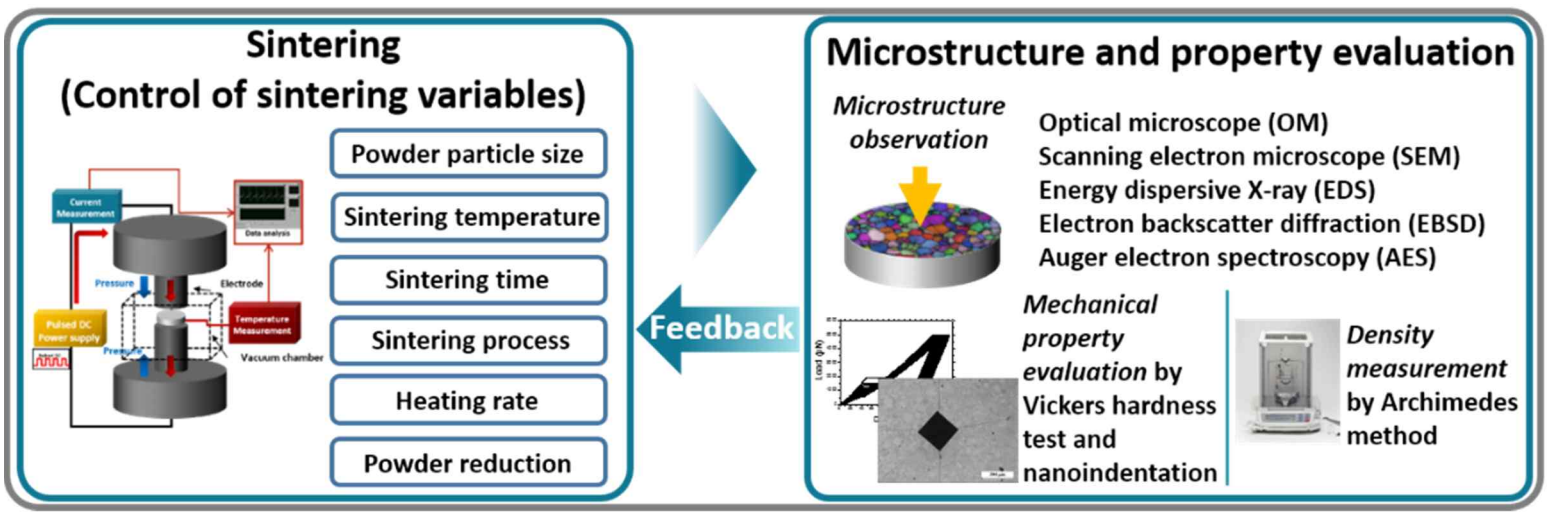

Figure 16. Experimental design to obtain high-density sintered tungsten.

3.3 Sample Preparations

After the sintering process, sintered tungsten samples were taken out from the graphite mold. A thick tungsten-carbide layer could be found in the top and bottom surface of the as-sintered tungsten samples, which is a result of reaction between the graphite mold and the tungsten powder. As tungsten carbide is a very hard material, it is difficult to grind tungsten carbide out by hand holding. To get rid of tungsten carbide layer on the top and bottom surface, sintered samples were held using specially designed stainless steel holders and ground with 60 grit SiC paper for 2 minutes on PH-3 (Allied), an auto-polishing device. The plate RPM and sample RPM were both 100 and the applied pressure was 27N. As contamination from the carbon sheet also occurred in the round of the sintered sample, round parts of samples were ground using 120 grid SiC paper for 15 minutes by hand polishing to remove all contaminated parts. Through these grinding process, samples showed a complete metallic glossy surface.

After grinding out all of contaminations in the samples, surface of samples were mirror polished for the microstructure observations. Also, Plansee ITER grade tungsten materials were also polished to be analyzed as a reference materials. Each sample was polished using 180, 320, 400, 600, 800 and 1200 grit SiC paper for 2, 2, 3, 5, 10 and 12 minutes respectively on the auto-polishing device PH-3. The platen RPM and sample RPM was 100 and the applied pressure was 27N. After polishing with the SiC paper, samples were further polished using diamond suspension and colloidal silica suspension (both

from Allied) using dilute DP-Lubricant Blue (Struers) using auto-polishing device PH-3. The polishing RPM was same as the polishing condition using SiC paper and the applied force was 17N. MD-Nap-T abrasive cloth (Struers) was utilized for subsequent polishing of 15 minutes using 6um and 1um diamond suspensions (Allied). After the diamond suspension polishing, samples were polished using colloidal silica having an average particle size of 20 nm for 15 minutes using an MD-chem (Struers) polishing cloth. After each polishing step, samples were ultrasonically cleaned in 99.9% ethanol for 2 minutes. The final dimensions of polished samples were diameter of about 10mm with thickness of about 3mm.

3.4 High Heat Flux Test

To test the thermal stability of the tungsten samples, a high heat flux (HHF) test was performed on the sintered samples and commercial ITER grade tungsten samples produced by Plansee AG. The heat loading test facility (SNU-HLT) (Figure 17) in Prof. Gon-Ho Kim's Laboratory in Seoul National University was utilized for the HHF test. HHF test is a common method to evaluate the thermal stability of materials for fusion applications. Under HHF loaded condition, materials with defects such as not-fully-sintered tungsten with pores could partially melt or boil and these could be a critical problem for the fusion applications.

The SNU-HLT is capable of applying the maximum heat flux of 10MW/m^2 [38]. It is known that the heat flux condition of KSTAR divertor is about 4.3 MW/m^2 and in the case of ITER divertor, the heat flux range is about 5 ~ 20 MW/m^2. Therefore, it was expected that the thermal stability of the sintered sample could be preliminary examined using SNU-HLT. In the HHF test, nitrogen plasma was utilized and the operating conditions of the device are as follows: Flowrate of 180 Slpm, applied current of 170A, plasma torch to sample distance of 5 and 7mm, test time of 300 second and coolant flowrate of 0.7lpm. The surface temperatures of the samples were measured using a 2-channel pyrometer and the amount of heat flux was calculated based on the temperature measured by thermocouples placed behind the sample inside the full-tungsten sample loading stage at 5 mm intervals. Depending on the

distance between the specimen and the torch, the surface temperature of the sample was set to 1400°C and 2300°C and the applied heat flux were about $3MW/m^2$ and $4MW/m^2$ respectively.

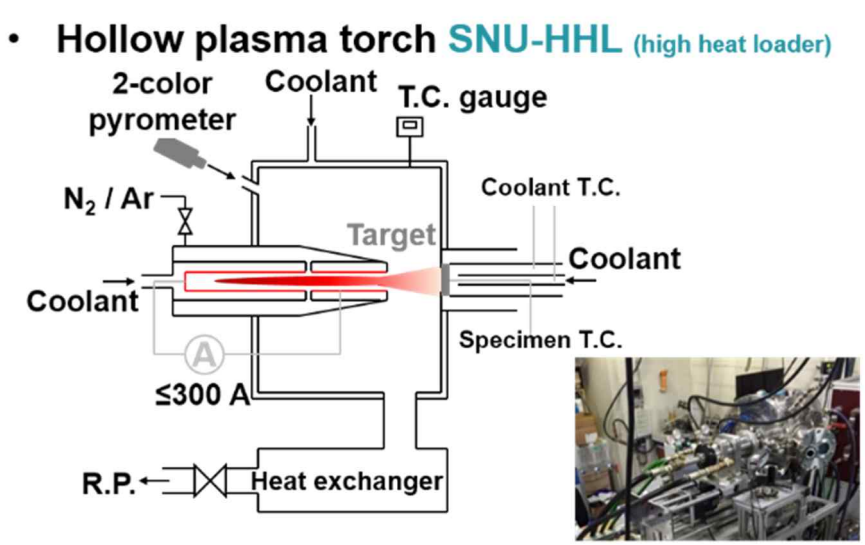

* for divertor components

Heat flux : ≤ 10 MWm^{-2}

** Relevant conditions **

- KSTAR Divertor: 4.3 MWm^{-2}
- ITER Divertor: 5~20 MWm^{-2}

Surface temp. : < 2500 ℃

- Two-color IR pyrometer

Active Cooling System

- P : 0.5 MPa, v : 0.9 m/sec,
- T: 300 K

** ITER cooling water condition **

pressure: 3.9 MPa, flow: 11 m/sec, temp : 340 K

Figure 17. Schematic diagram of high heat flux test machine and its specification [38].

3.5 Microstructure Observations and Property Measurements

For the microstructure observations, Optical microscope (Canon), FE-SEM (Hitach, SU-70) with EBSD (EDAX, Hikari) and EDS (X-Max50, Horiba) was utilized. FE-SEM was observed using accelerating voltage of 15kV with working distance of 15mm. 'TSL OIM Analysis 6' was used for the EBSD analysis. Both FE-SEM and EBSD images were taken at magnification of 1000 times with a step size of 0.3μm. The grain was defined to possess at least misorientation angle of 15°.

To see the impurity contents in the grain boundaries, AES (PHI660 in KIST) was used in this study. AES is an effective method to detect elements consisting surface of a sample. By in-situ fracturing of the samples in the AES vacuum chamber, intergranular fractured surface was revealed and the impurity contents on the grain boundaries were confirmed. AES was observed using accelerating voltage of 3kV and the sputtering rate was 33Å SiO_2/min for the sintered sample and 10Å SiO_2/min for the recrystallized Plansee ITER grade tungsten sample.

For the property measurements, hardness values were acquired by Vickers hardness test device (430SVD, Wolpert group) and relative densities were calculated using Archimedes method. The theoretical density of tungsten was set to 19.25g/cm^2. Vickers harness test was conducted under HV30 and

Archimedes method was conducted using distilled water and scale (AP210, OHAUS). For both measurements, mean values were obtained from 5 times of measurements.

3.6 High Temperature Reduction

For all of the sintered samples, intergranular cracking behavior was observed during indentation by Vickers hardness test. To solve this problem, high temperature compression test was conducted under 680°C (Figure 18). Compressed samples were mirror polished round shaped high-density sintered tungsten samples and their initial thickness was about 3.0mm. The high temperature compression test was conducted using tensile/compression test machine (5900R5582, Instron) with furnace (SF-16 2300, Instron) and the compression speed was 0.05mm/second. The reduction was conducted to reduce sample thickness of 10% to 20%.

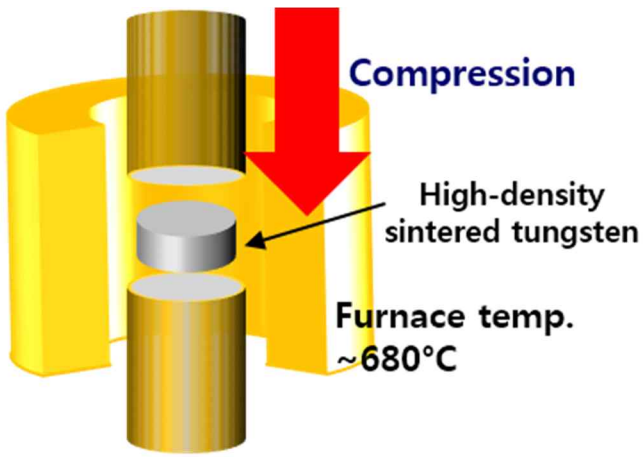

Figure 18. Schematic diagram of high temperature reduction of sintered tungsten.

4. Results and discussion

4.1 Fabrication Process and the Microstructure of ITER grade W material

Before beginning the sintering, commercial tungsten materials for fusion application was analyzed. Through report paper about ITER application materials, the manufacturing process of ITER grade tungsten materials were obtained [1]. According to the paper, tungsten powder is produced by H_2 reduction of tungsten oxide which was obtained from ammonium paratungstate. Then the tungsten powder is compacted at room temperature to make a green compact and sintered in a sintering furnace at temperatures of above 2200°C to produce a sintered tungsten having relative density of about 80%. Sequentially, sintered tungsten undergo a thermo-mechanical process to achieve relative density of 99.9% and heat-treated for the stress-relief. These process was also confirmed by a meeting with the head of market unit material technologies of Plansee who was in charge of fabrication of Plansee ITER grade tungsten materials (Plansee-W).

Tungsten mono-block made for ITER divertor application (Plansee made) was obtained and analyzed in its microstructures and properties. The mono-block was high-temperature rolled tungsten. Since there are some reports that the developed direction of the grains in tungsten materials may influence the performance of material [39,40], two kinds of samples were made according to

the grain developed direction to the surface: samples with parallel developed grain (Plansee-W_p) and samples with normally developed grain (Plansee-W_n). (Figure 19) These developed trend was originated from the thermomechanical process.

Figure 20 shows the results of microstructure observations of Plansee-W_p and Plansee-W_n. In Plansee-W_p, the elongated grains were observed and the average grain size was 13.3μm. In Plansee-W_p, the preferred oriented grains were observed and the average grain size was 4.3μm. Through misorientation profiling (Figure 21), it is obviously shown that the portion of low angle grain boundaries (<10°) is dominant and the distribution of rest of angle grain boundary does not follow random distribution. All of these microstructural characteristics are originated from thermo-mechanically process. Also, some amount of pores are observed in both Plansee-W_p and Plansee-W_n (Figure 22).

Through Vickers hardness test, Plansee-W_p was confirmed to have hardness of about 392HV30 with standard deviation (STDEV) of 3HV and for Plansee-W_n, hardness was about 390HV30 with STDEV of 4HV. By Archimedes methods, both samples shown relative density of about 99.9%.

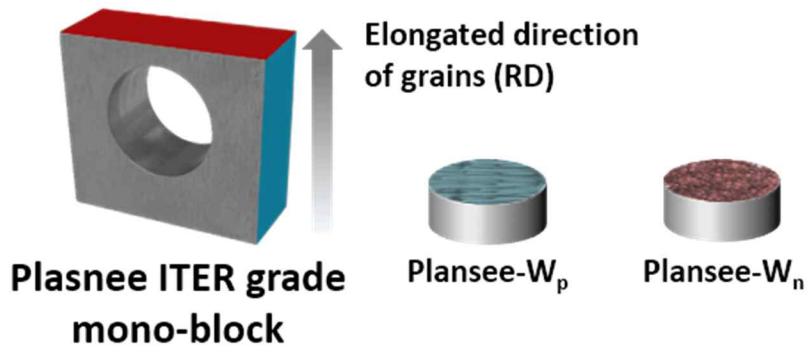

Figure 19. Shape of Plansee ITER grade tungsten mono-block and samples with parallel developed and normally developed grains.

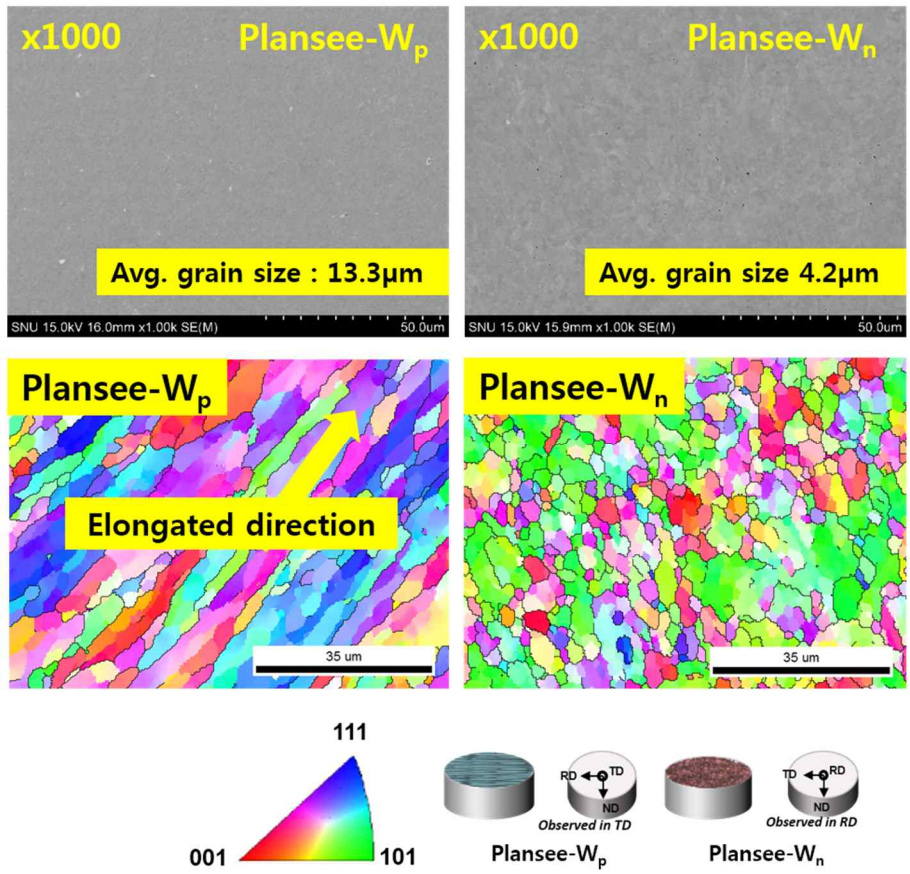

Figure 20. SEM and EBSD inverse pole figure map observations of Plansee ITER grade W samples.

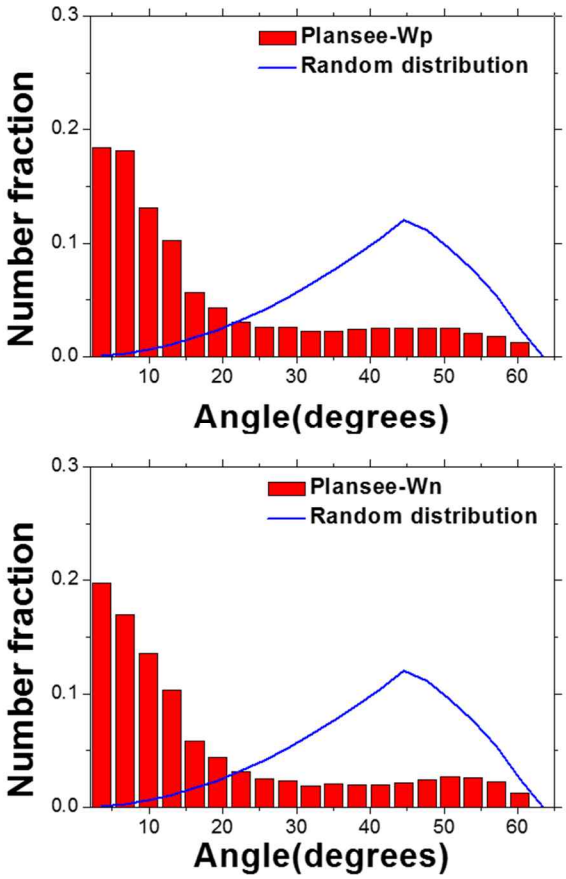

Figure 21. Misorientation angle profiles of Plansee ITER grade W samples.

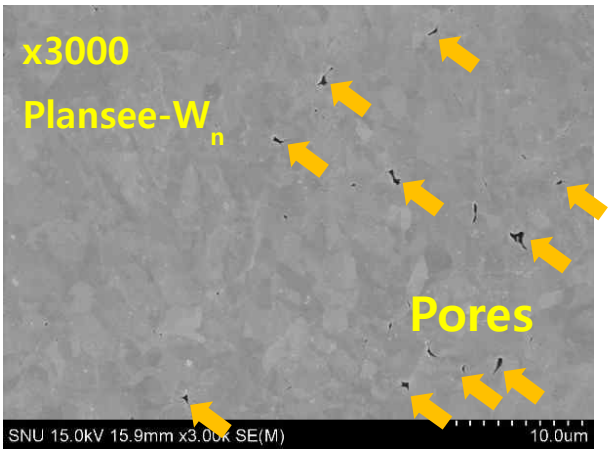

Figure 22. Pores in Plansee ITER grade tungsten samples.

4.2 Effect of Sintering Factors in Spark Plasma Sintering

In this study, SPS was utilized to fabricate high-density sintered tungsten samples. The density of sintered material is affected by various factors such as sintering powder size, sintering time, sintering temperature, sintering process, heating rate and powder reduction treatment. In order to obtain sintering conditions for high-density sintered tungsten samples, aforementioned sintering factors were independently controlled and their effects were investigated.

4.2.1 Effect of the Powder Particle Size

In order to investigate the effect of the powder particle size in sintering, tungsten powders having an average particle size of 4.8μm, 2.4μm and 0.5μm were respectively sintered using single step sintering process for 5 minutes at 1500°C with heating rate of 100°C/min and under a pressure of 25MPa. The microstructure of sintered samples was observed using OM (Figure 23). As a result, it was confirmed that size of the pores in the sintered material (dark area in Figure 23) decreased with decreasing particle size. This result is in agreement with the conventional knowledge that the smaller powder particle is beneficial for the densification of material as smaller powder particle size means a larger the surface energy which is a driving force of sintering. As a result, it can be concluded that the smaller particle size of the tungsten powder is advantageous for sintering. From this, tungsten powder having an average particle size of 0.5μm, which is the smallest particle size of commercially available powder, was used in the study.

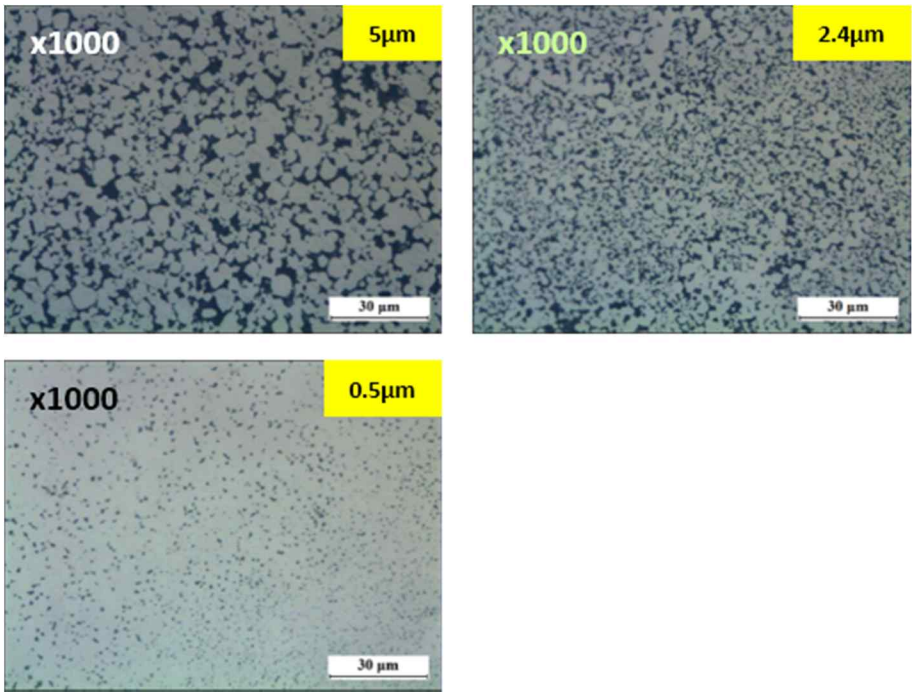

Figure 23. Microstructures of sintered tungsten samples using different sizes of powders.

4.2.2 Effect of the Sintering Temperature

In order to investigate the effect of sintering temperature in sintering, tungsten powder having an average particle size of 0.5μm was sintered using single step sintering process for 10 minutes at 1300°C, 1400°C, 1500°C, 1600°C respectively with heating rate of 100°C/min and under a pressure of 35 MPa. The relative density of each sintered sample was measured to be 95.5%, 96.3, 97%, and 96% respectively by Archimedes method. The average grain size of samples was 2μm, 3.5μm, 9μm, and 9.6μm, respectively. From the SEM/EBSD observations (Figure 24), it was found that the average grain sizes of the sintered samples were increased with increasing sintering temperature. However, the density of samples did not increase above some level of sintering temperature. This result indicates that the optimization is required to achieve the high-density sintered tungsten.

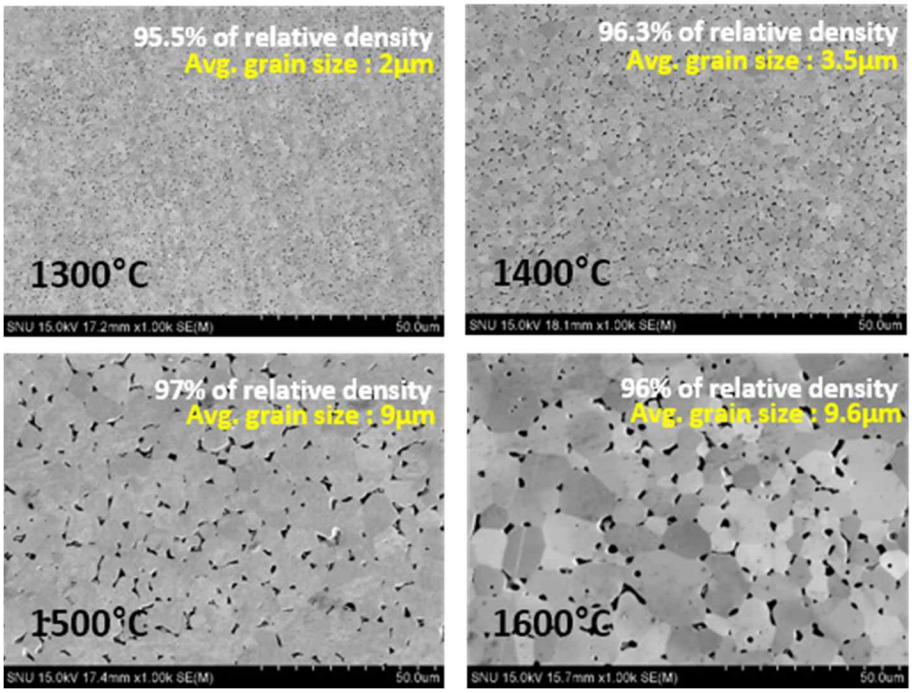

Figure 24. Microstructures of sintered tungsten samples using different sintering temperature.

4.2.3 Effect of the Sintering Time

In order to investigate the effect of sintering time in sintering, tungsten powder having an average particle size of 0.5μm was sintered using single step sintering process for 5 and 10 minutes respectively at 1600°C with heating rate of 100°C/min and under a pressure of 35 MPa. As a result, the average grain sizes of samples were 5.3μm and 9.6μm respectively, showing that the grain growth occurred in proportion to the sintering time (Figure 25). The relative density was 96% and 95% respectively. It was found that the increase in sintering time induced grain growth, but did not significantly affect the density. As a result, it was confirmed that sintering time of 5 minutes may be enough for the densification and for the control of microstructure such as grain size, optimization of sintering time is required.

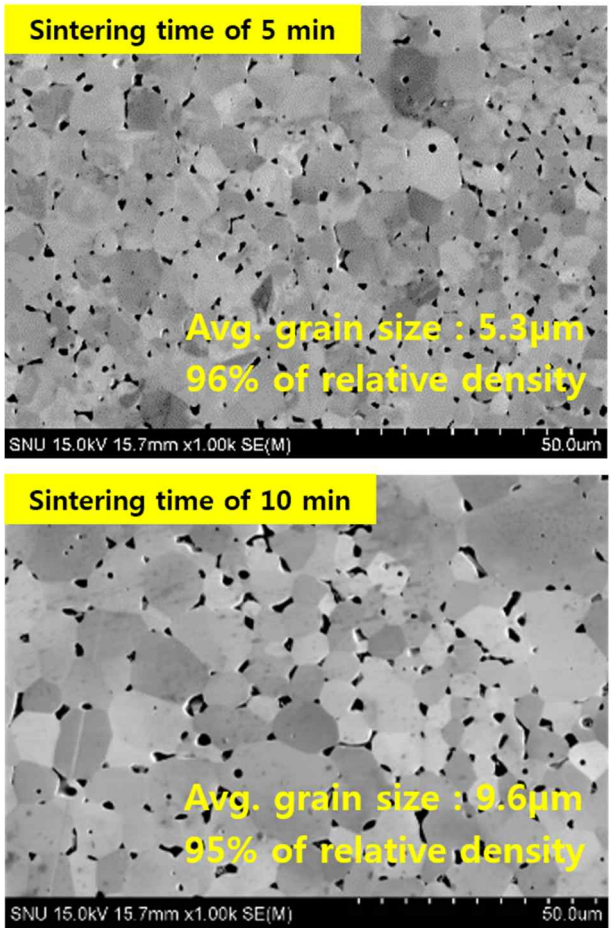

Figure 25. Microstructures of sintered tungsten samples using different sintering time.

4.2.4 Effect of the Sintering Process

In order to investigate the influence of the sintering process, powder having an average particle size of 0.5μm was respectively sintered using single step and two step sintering (TSS). The TSS is a sintering process consisting of two sintering temperatures, which requires rapid heating and cooling rates during sintering thus is advantageous to apply in SPS. It is known that at the T_1 of the TSS, large pores are removed and the necks which is the bonding between the powders are formed. At the T_2, densification avoiding grain coarsening is known to take place [42].

The sintering temperature was 1600°C for the single step sintering and for TSS, T_1 was 1600°C and T_2 was 1300°C. The time interval of T_1 to T_2 was 10 seconds and the sintering time was counted when the temperature reached T_2. The heating rate was 100°C/min and sintering time was 5 minutes for both sintering conditions. Pressure of 30MPa was also applied for both conditions. Through microstructure observations (Figure 26), it was confirmed that the pores at the surface of the sintered tungsten were drastically reduced by the TSS. The average grain sizes were 5.3μm and 3.6μm respectively, and the relative density was 96% and 97.4% respectively. This correspond with the known effect of TSS [42] that retardation of grain growth and densification occur during TSS. As a result, it was concluded that the TSS is advantageous for fabrication of high-density sintered tungsten samples having a smaller average grain size and higher density than the single step sintered tungsten samples.

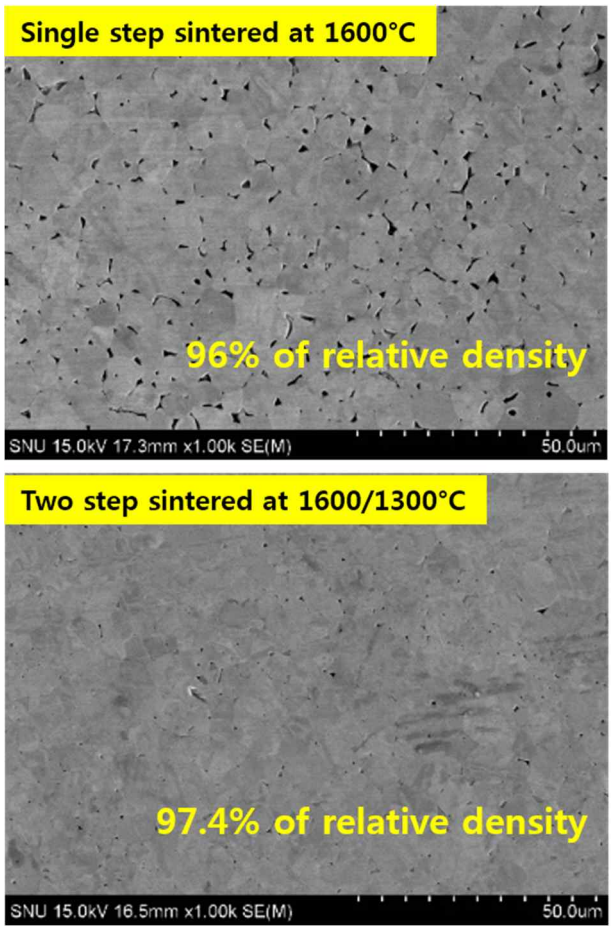

Figure 26. Microstructures of sintered tungsten samples using different sintering process.

4.2.5 Effect of the Heating Rate

In order to investigate the effect of the heating rate, tungsten powders with an average particle size of 0.5μm were sintered for 5 minutes with different heating rate. The heating rates were set as 50°C /min and 100°C/min respectively using TSS with T_1 of 1600°C and T_2 of 1300°C. The microstructure of each samples are shown in Figure 27. Though there were no big differences shown in SEM observations, their density differed depending upon heating rate. The relative density of the sintered sample with a heating rate of 100°C/min was measured to be 97.5%, and the sample with a heating rate of 50°C/min had a relative density of 98.5%. As a result, it was confirmed that under given TSS condition, heating rate of 50°C/min was favorable to obtain high-density sintered tungsten samples.

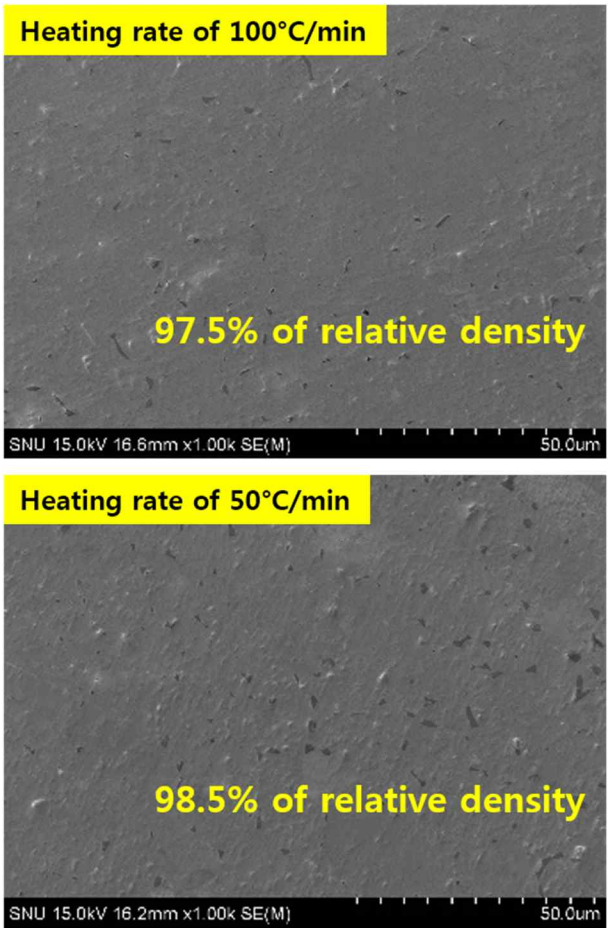

Figure 27. Microstructures of sintered tungsten samples using different heating rate.

4.2.6 Effect of the H_2 Reduction

In the sintered samples fabricated using as-received powder, high-oxygen contents area was revealed by EDS point scan (Figure 28). As tungsten is easily oxidized, it was suspected that these high-oxygen contents area originated from the tungsten oxide layer in the as-received tungsten powder, rather than from the oxides formed during the sintering process. From the meeting with the head of market unit material technologies of Plansee AG, it was confirmed that the Plansee AG adopted continuous H_2 reduction and sintering process for production of ITER grade tungsten materials. This indicate that the tungsten powder used for commercial product does not have any chances to be exposed to air thus will not have any oxide layer on the surface of the powder particle. Considering the manufacturing conditions of Plansee ITER grade tungsten materials, the tungsten powder used in this study would possess the oxide layer on the surface of powder particle even though the powders were kept in the vacuum desiccator**.** As such oxygen layer may contribute to the formation of the high-oxygen contents area but also act as a diffusion barrier in sintering, H_2 reduction of tungsten powder was considered. The reduction conditions of tungsten oxide (WO_3) under 100% H_2 atmosphere were calculated (Figure 12) using FactSage, a commercial thermodynamic calculation program. As a result, it was confirmed that the reduction of tungsten oxide could take place at temperature above 830°C.

In order to investigate the influence of powder reduction, TSS was conducted using the as-received powder and test reduced powder which was reduced under 1300°C for 2 hours in 5% H_2 and 95% Ar atmosphere. Average particle sizes of both powders were 0.5μm. Powders were sintered for 10 minutes at T_1 of 1700°C and T_2 of 1400°C with heating rate of 100°C/min under a pressure of 60 MPa.

The relative density of the sample using the as-received powder was 97.3% and the relative density of the sample using reduced powder was 99.5%. The average grain size was 17.4μm and 5.5μm respectively. Also, it was found that the high-oxygen contents area was barely observed in the sintered sample using the reducing powder (Figure 29). As a result, it was confirmed that sintered tungsten samples with a smaller grain size and a higher density can be obtained using reduced powder. Also, it was expected that if the powder was reduced in a 100% H_2 condition, oxygen contents in the as-received powder would decrease much more comparing to the reduced powder reduced under the 5% H_2 and 95% Ar atmosphere, making it easier to obtain high-density sintered tungsten samples.

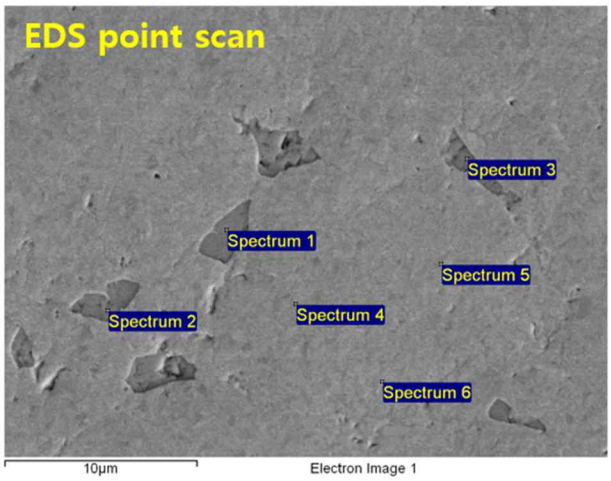

Spectrum	C	O	W	Total
Spectrum 4	4.06	0.56	95.38	100.00
Spectrum 5	3.80	0.40	95.79	100.00
Spectrum 6	3.52	0.57	95.91	100.00
Spectrum 1	3.03	15.25	81.72	100.00
Spectrum 2	3.18	15.60	81.21	100.00
Spectrum 3	2.62	15.18	82.20	100.00
Mean	3.37	7.93		
Std. deviation	0.53	8.13	7.67	

dark-colored area

Figure 28. EDS point scan results of sintered samples.

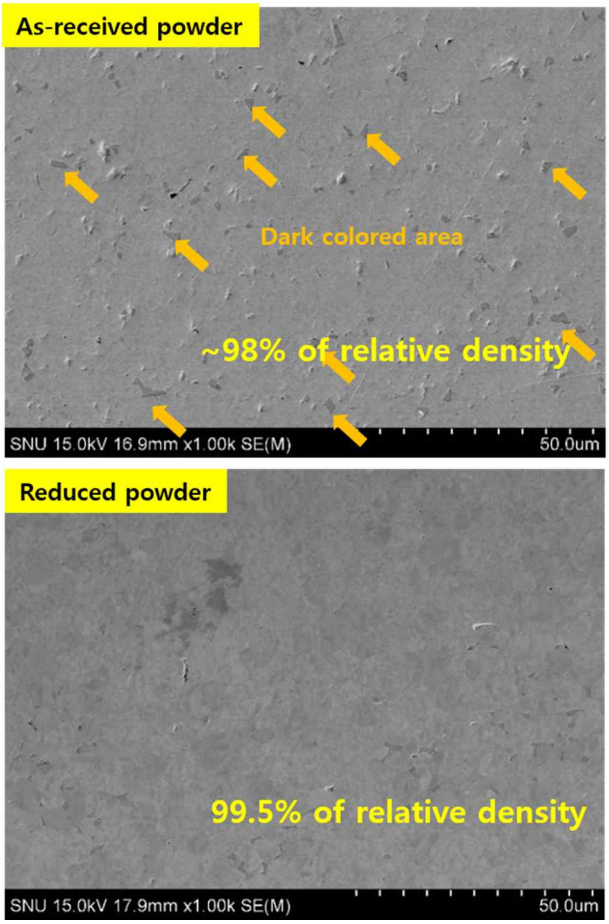

Figure 29. Microstructures of sintered tungsten samples using as-received and reduced powders.

4.3 Optimized Sintering Conditions for High Densification

Considering the effects of the sintering factors, it can be deduced that the high-density sintered tungsten samples could be obtained with TSS using reduced powder. To fully reduce the tungsten powder, as-received tungsten powder having an average particle size of 0.5μm was reduced under two 100% H_2 atmosphere conditions: at 900°C for 24 hours and at 1100°C for an hour.

Using obtained reduced powders, three kind of high-density sintered tungsten samples with relative density of 99.9% named SPS-W_1, SPS-W_2 and SPS-W_3 were successfully fabricated. Also, two kind of optimized sintering conditions were obtained. One optimized sintering condition was TSS with T_1 of 1700°C and T_2 of 1400°C using heating rate of 100°C/min under pressure of 60MPa and the sintering time was 5 minutes. One optimized sintering condition was TSS with T_1 of 1600°C and T_2 of 1300°C using heating rate of 50°C/min under pressure of 60MPa and the sintering time was 5 minutes. Table 1 shows the sintering conditions, powder reduction conditions, average grain sizes, relative density and hardness of high-density sintered samples. Figure 30 shows the microstructure of the high-density sintered tungsten samples. The sintered tungsten samples were found to have less porosity on the surface having average grain sizes of about 2.0 to 4.0μm and a relative density of 99.9%. Through misorientation angle profile (Figure 31), it can be seen that the high

angle grain boundaries follows random distribution. Hardness values of sintered samples were found to be about 350 to 370HV30.

Sample name	Powder reduction conditions	Sintering conditions (Spark plasma sintering)	Relative density	Average hardness (STDEV)	Average grain size
SPS-W$_1$	100% H_2 reduced (**900°C** 24H) 0.5µm	Two step sintering 1600-1300, 50°C/min 60MPa, 5min	**99.9%**	370HV30 (3)	2.1 µm
SPS-W$_2$	100% H_2 reduced (**1100°C** 1H) 0.5µm			359HV30 (6)	4.0 µm
SPS-W$_3$		Two step sintering 1700-1400, 100°C/min 60MPa, 5min		352HV30 (4)	4.4 µm

Table 1. Sintering conditions and properties of high-density sintered tungsten samples.

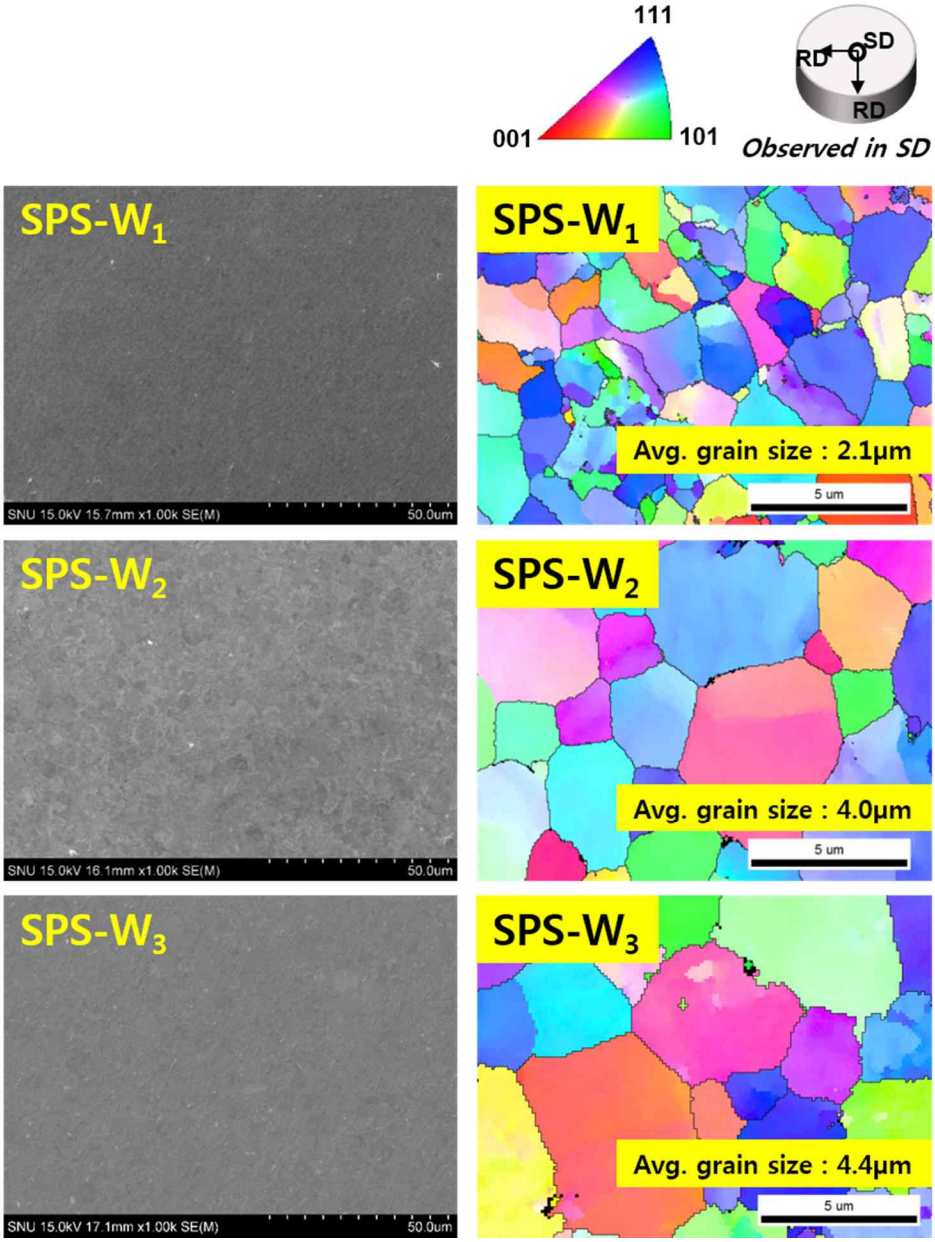

Figure 30. Microstructures of high-density sintered tungsten samples by SEM and EBSD inverse pole figure map.

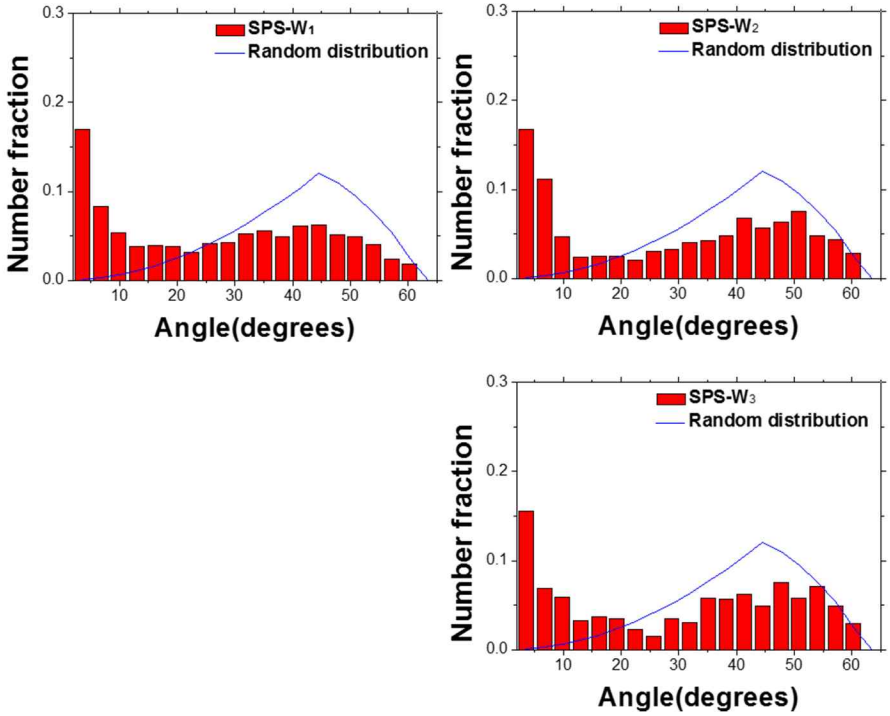

Figure 31. Misorientation angle profiles of high-density sintered tungsten samples.

4. 4 Thermal Stability of W Samples

Fabricated high-density sintered tungsten samples (SPS-W_1 and SPS-W_3) were high heat flux (HHF) tested using SNU-HLT (Thermal Loading Test Facility) in Prof. Gon-Ho Kim's laboratory, Seoul National University. To evaluate the performance of the sintered samples, Plansee-W_p, Plansee-W_n and not-fully-sintered tungsten samples (SPS-W_{nfs}) with relative density of 98% were also HHF tested as reference materials.

Two sets of HHF test were conducted changing surface temperature of samples to reach 2300°C and 1400°C. Amount of heat flux passing samples were about 4MW/m^2 for the surface temperature of 2300°C and 3MW/m^2 for the surface temperature of 1400°C. The SPS-W_3 and Plansee-W_n were tested under both 2300°C and 1400°C surface temperature conditions and SPS-W_1, SPS-W_{nfs} and Plansee-W_p were only tested under 2300°C surface temperature condition.

Through SEM and EBSD images of before and after HHF test, the changes in surface morphology, grain size and misorientation distribution were observed. Also, hardness changes were measured by Vickers hardness test.

Figure 32 shows the surface of HHF tested SPS-W_{nfs}. In the SEM images, many severely damaged regions were observed. As not-fully-sintered means high porosity of the sintered material, this could be one reason for the partial

melting on the surface due to its degraded thermal conductivity causing heat accumulation on the surface.

Figure 33 shows the surface of Plansee-W_p and Plansee-W_n under the condition of surface temperature of 2300°C. In the SEM images, it can be observed that the mirror polished surface became a rough surface. These surface morphology changes seem to originate from the grain boundary grooving of tungsten materials. [41] Also, there were no severely damaged region at the sample surface. Through EBSD observations (Figure 34), the huge grain growth was observed in Plansee-W_n. The average grain size of Plansee-W_n before HHF test was 4.2μm and after HHF test, the average grain size of Plansee-W_n was 35.3μm, showing about 9 times of grain growth after HHF test. For Plansee-W_p, the average grain size was grown about 2 times, from 13.3μm to 29.6μm. Through misorientation profiling (Figure 35), it is seen that both Plansee-W samples were recrystallized as the misorientation distributions well follow the random distribution. The hardness test results also supports that the HHF tested Plansee-W samples were recrystallized. Before HHF test, hardness of Plansee-W_p and Plansee-W_n were about 390HV30. After HHF test, the hardness of Plansee-W_p was 316HV30 with STDEV of 2HV and hardness of Plansee-W_n was 303HV30 with STDEV of 3HV, dropping their hardness more than 70HV.

Figure 36 shows the surface of SPS-W_1 and SPS-W_3 under the condition of surface temperature of 2300°C. In the SEM images, it can be observed that both

mirror polished surfaces became rough surfaces. Also, there were no severely damaged region at the both samples like Plansee-W materials. Through EBSD observations (Figure 37), the grain growth was observed in both samples. Before HHF test, the average grain sizes of SPS-W_1 and SPS-W_3 were 2.1μm and 4.4μm respectively. After HHF test, the average grain sizes of SPS-W_1 and SPS-W_3 were 6.0μm and 6.4μm respectively, showing about 2 to 3 times of grain growth. Through misorientation profiling (Figure 38), it is seen that both samples possess recrystallized microstructure as the misorientation distributions well follow the random distribution. Through hardness test results, it was confirmed that the SPS-W samples possess stable mechanical property than Plansee-W samples. Before HHF test, hardness of high-density sintered samples were about 352~370HV30. After HHF test, the hardness of SPS-W_1 was 330HV30 with STDEV of 3HV and the hardness of SPS-W_3 was 326HV30 with STDEV of 3HV, dropping their hardness about 30~40HV.

Figure 39 shows the sample surface of SPS-W_3 and Plansee-W_n under the condition of surface temperature of 1400°C. Through the SEM images, changes in surface morphology were observed and there were no severely damaged region in both samples. In Plansee-W_n, average grain size were increased about 6 times after HHF test, from 4.2μm to 24.7μm. However, in SPS-W_3, average grain size were slightly changed after HHF test. The average grain size before HHF test was 4.4μm and those after HHF test was 3.4μm (Figure 40). Considering that the average grain size was obtained by EBSD observation

which observes very small area of sample, it could be said that the grain size barely changed. Through misorientation profiling (Figure 41), it is seen that both samples possess recrystallized microstructure as the misorientation distributions well follow the random distribution. The stability of SPS-W_3 under HHF condition was also confirmed by hardness changes. Before HHF test, hardness of SPS-W_3 and Plansee-W_n were about 371HV30 and 392HV30 respectively. After HHF test, the hardness of samples were about 378HV30 with STDEV of 2HV and 332HV30 with STDEV of 6HV respectively. From the hardness test result, it was confirmed that the hardness of SPS-W_3 slightly changed but the hardness of Plansee-W_n decreased about 60HV. Considering the operating temperature of the fusion reactor, stable microstructure and mechanical property of SPS-W_3 under condition of surface temperature of 1400°C is remarkable.

From the HHF test results, it seems that the high-density sintered tungsten samples (SPS-W_1 and SPS-W_3) possess much stable microstructure at the high temperature comparing to the Plansee-W samples (Plansee-W_p and Plansee-W_n). It seems that the thermal stability of high-density sintered tungsten samples is originated from its fabricated process. The absence of thermo-mechanical process in the fabrication process of high-density sintered tungsten samples would be beneficial to the thermal stability. In Plansee-W samples, driving force for recrystallization and grain growth would be bigger than that of the high-density sintered tungsten materials as Plansee-W samples had

undergone thermo-mechanical processes thus possess much residual stresses and strains inside. Also, as high-density sintered tungsten samples were as-sintered samples sintered under temperatures ranging 1300~1700°C, their microstructures might be stabilized in such temperature.

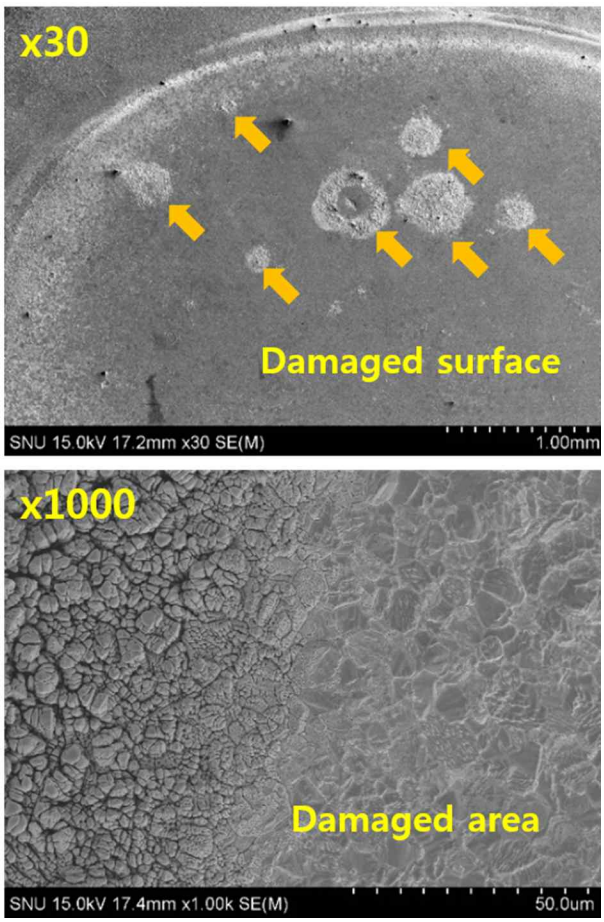

Figure 32. Damaged surface of HHF tested SPS-W_{nfs} (at surface temperature of 2300℃).

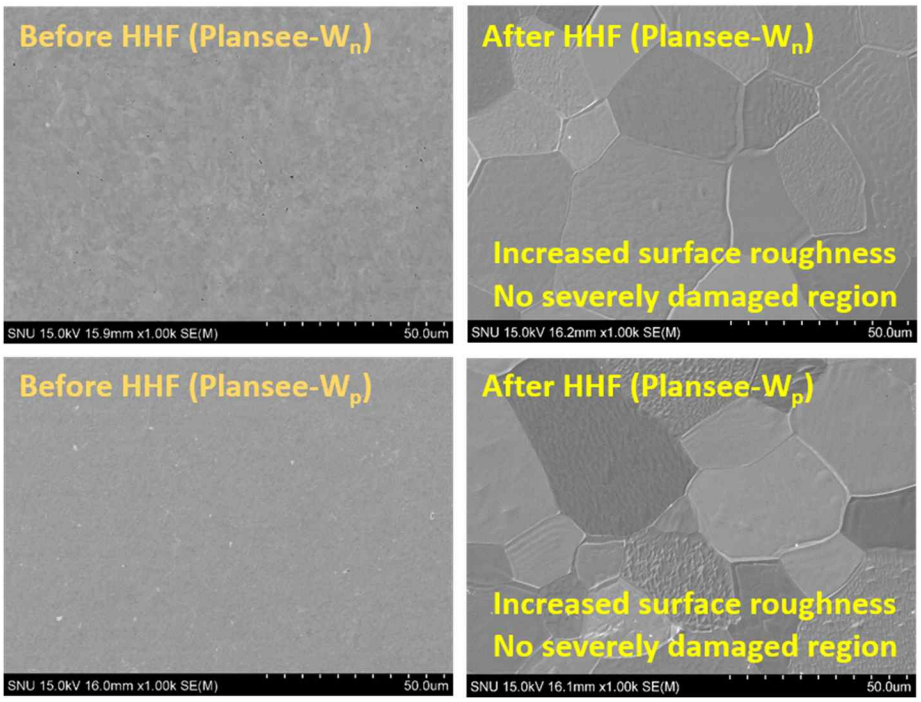

Figure 33. Microstructures of Plansee ITER grade W samples before and after high heat flux test (at surface temperature of 2300°C).

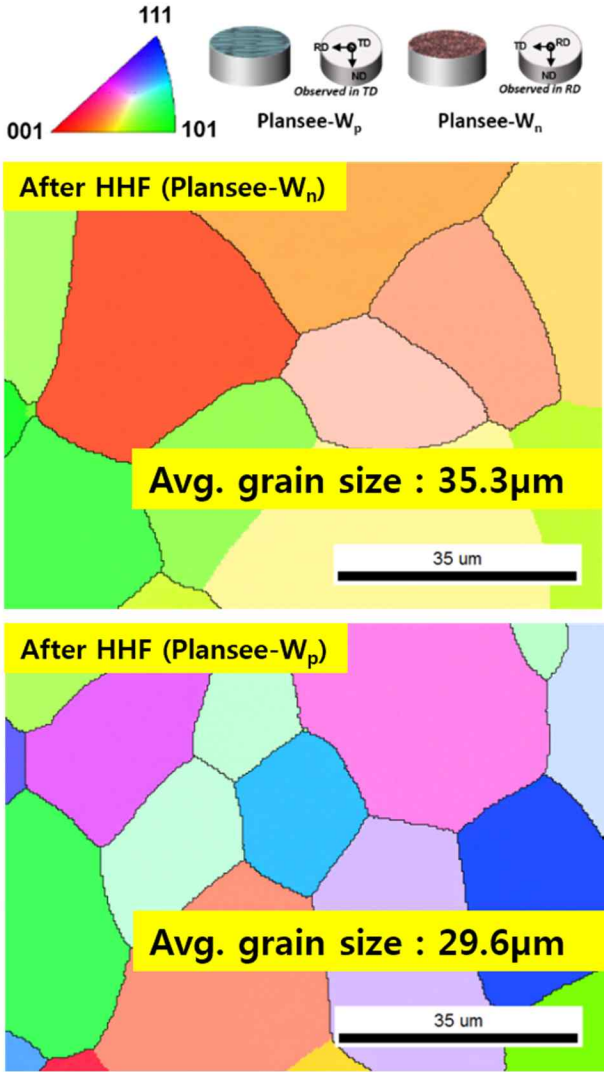

Figure 34. EBSD inverse pole figure maps of Plansee ITER grade W samples after high heat flux test (at surface temperature of 2300°C).

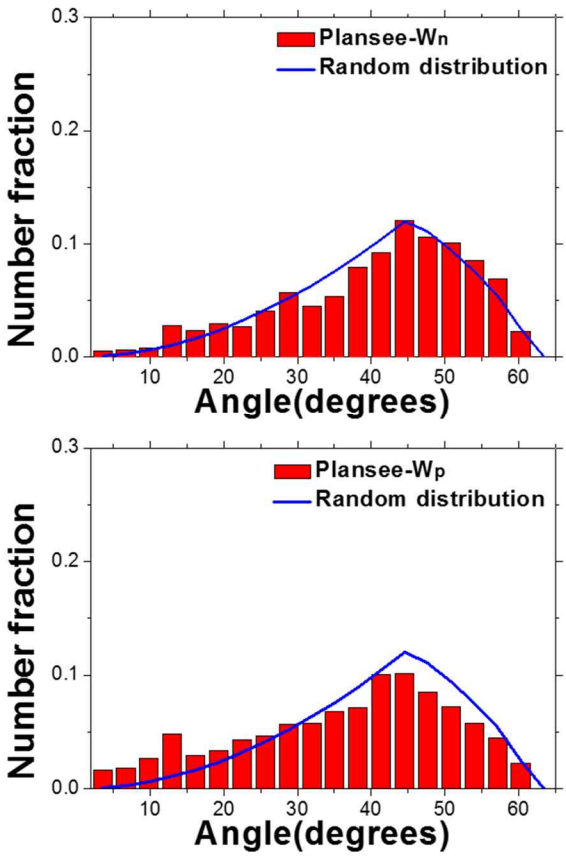

Figure 35. Misorientation angle profiles of Plansee ITER grade W samples after high heat flux test (at surface temperature of 2300°C).

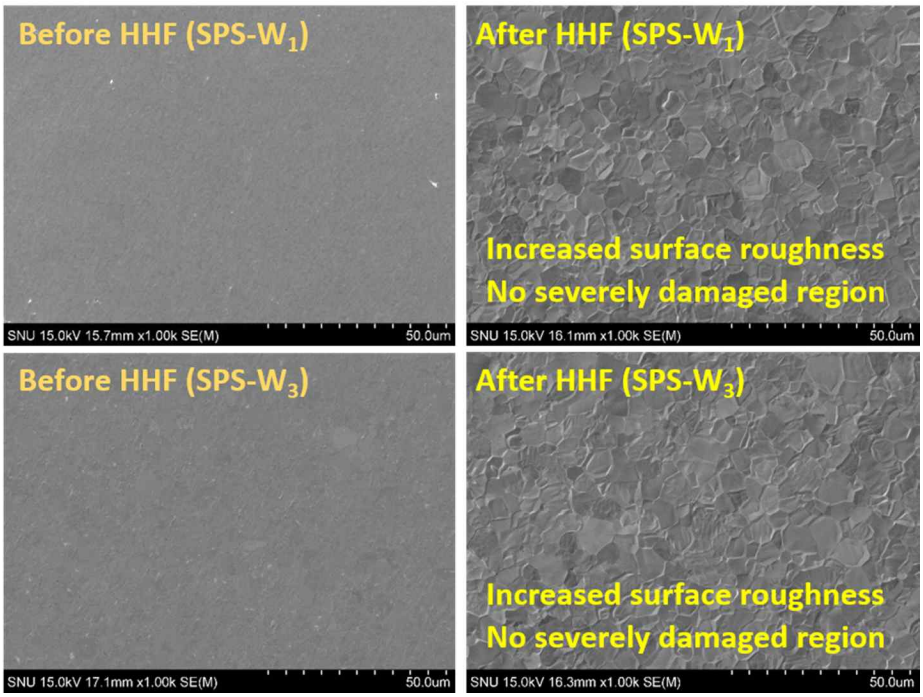

Figure 36. Microstructures of high-density sintered W samples before and after high heat flux test (at surface temperature of 2300°C).

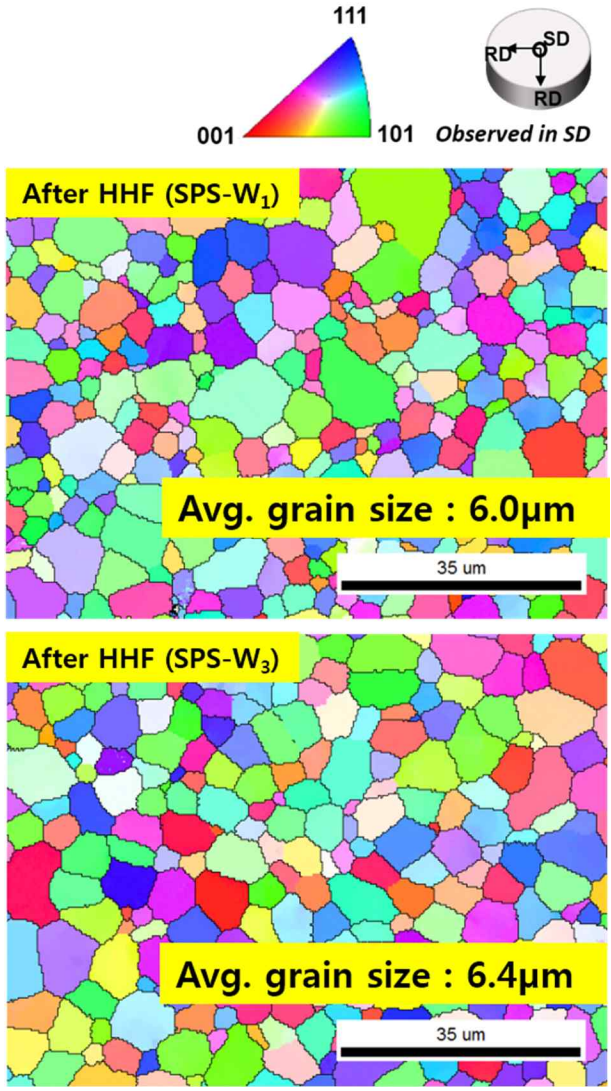

Figure 37. EBSD inverse pole figure maps of high-density sintered W samples after high heat flux test (at surface temperature of 2300°C).

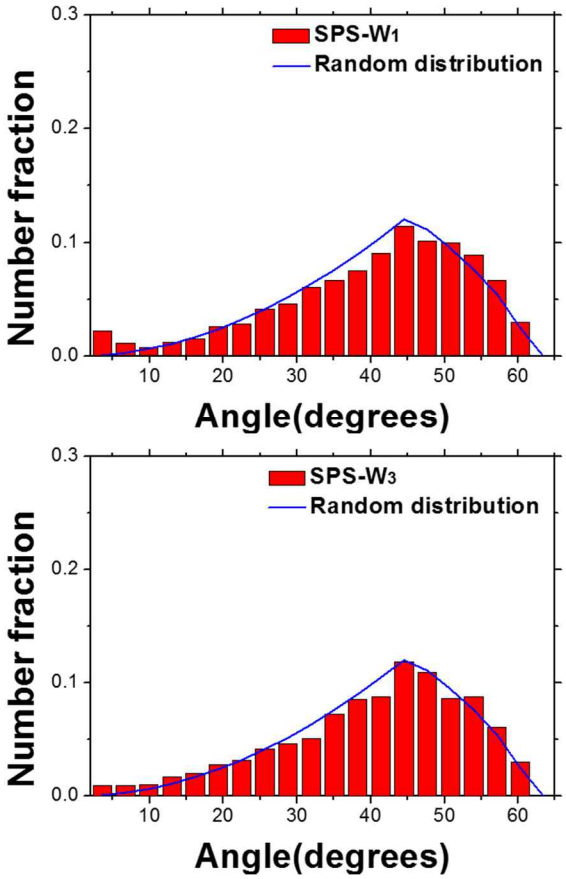

Figure 38. Misorientation angle profiles of high-density sintered W samples after high heat flux test (at surface temperature of 2300°C).

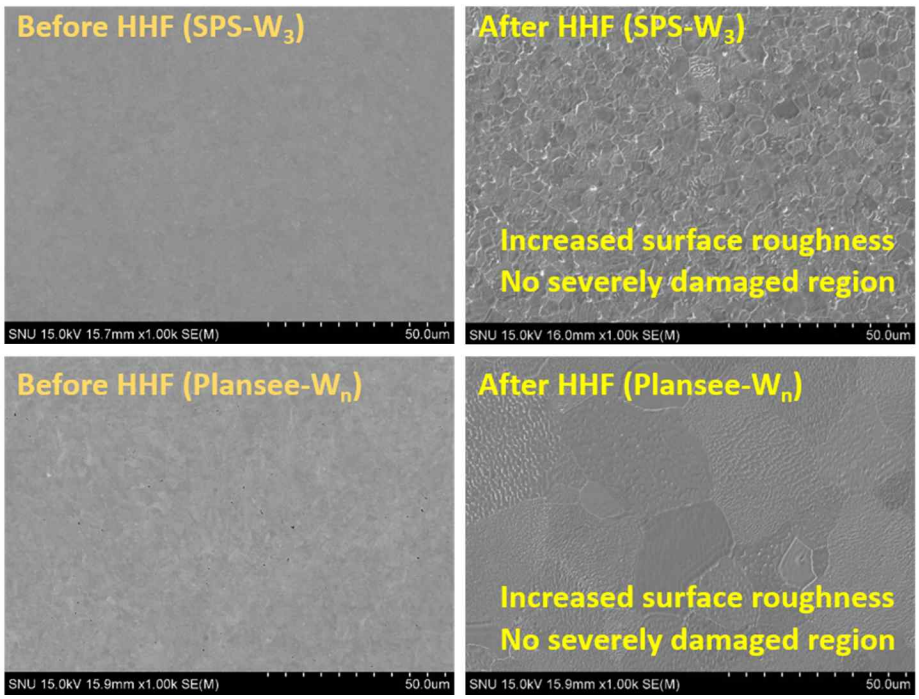

Figure 39. Microstructures of SPS-W_3 and Plansee-W_n before and after high heat flux test (at surface temperature of 1400℃).

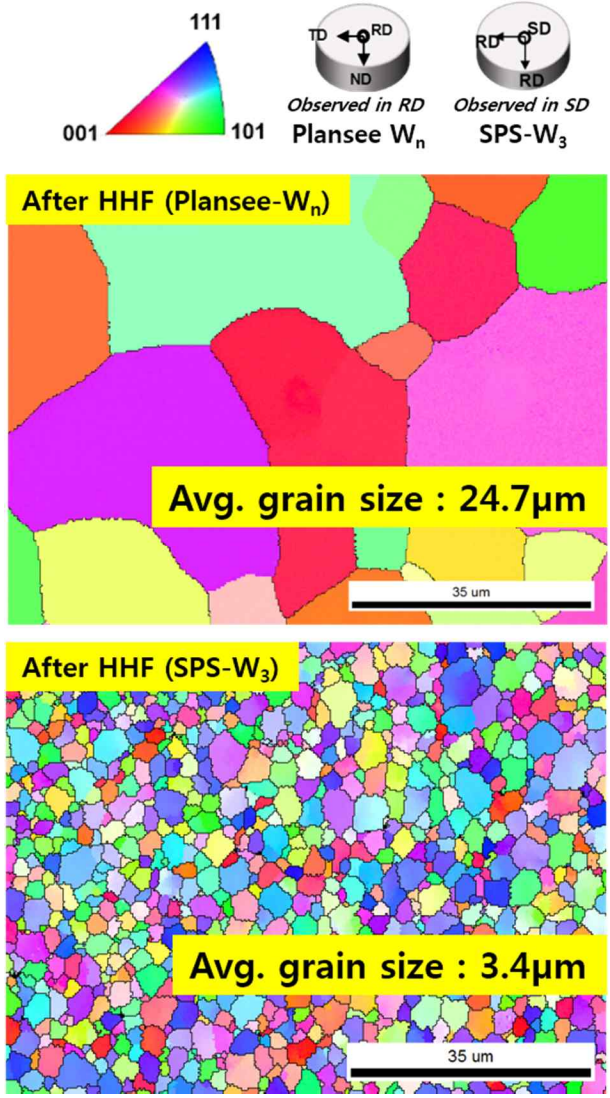

Figure 40. EBSD inverse pole figure maps of SPS-W_3 and Plansee-W_n after high heat flux test (at surface temperature of 1400°C).

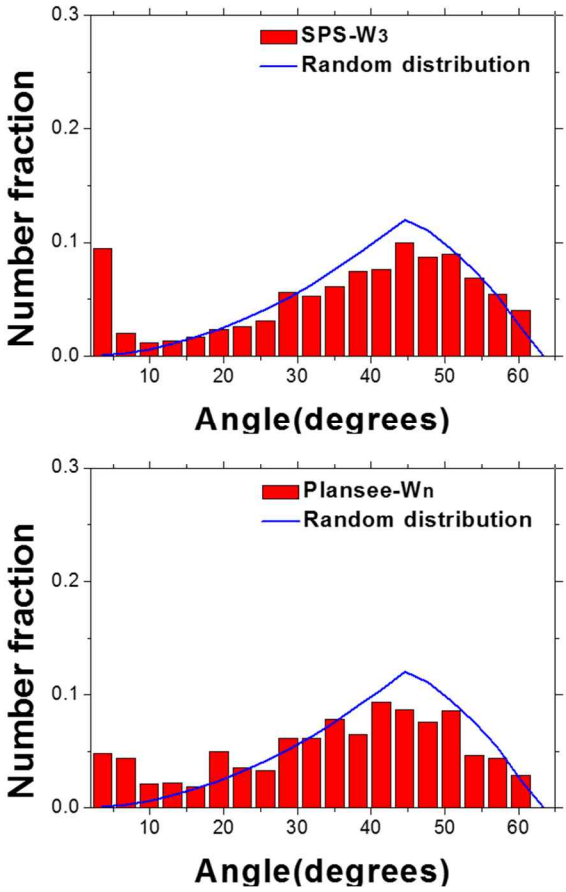

Figure 41. Misorientation angle profiles of SPS-W_3 and Plansee-W_n after high heat flux test (at surface temperature of 1400°C).

4.5 Improvement of Mechanical Property of the Sintered Samples

In this study, high-density sintered tungsten samples with relative density of 99.9% were fabricated using SPS without thermo-mechanical process. However, cracks were observed after Vickers hardness test in the high-density sintered tungsten samples which were not observed in Plansee-W (Figure 42). By correlating SEM and EBSD observations (Figure 43), it was revealed that those cracks in SPS-W were all intergranular cracking. Tungsten is known to exhibit brittle behavior at room temperature due to its high ductile brittle transition temperature (DBTT, above 250°C, changes depending upon the amount of deformation). However, such brittle behavior did not observe in Plansee-W after indentation.

The difference between the Plansee-W and high-density sintered tungsten samples is the manufacturing process. As Plansee-W had undergone thermo-mechanical process, residual stress may exist in the material and its microstructure is affected showing elongated or preferred oriented grains (Figure 20). To confirm the effect of thermo-mechanical process on the brittle behavior of SPS-W, recrystallized Plansee-W (Plansee-W_{rx}) and reduced high-density sintered tungsten samples (SPS-W_r) were prepared. Plansee-W_{rx} was obtained by heat-treating as-received Plansee-W at 1500°C with 5% H_2 and 95% Ar atmosphere for the recrystallization. SPS-W_r were obtained by compressing

SPS-W about 10~20% at 680°C (Figure 18). Plansee-W_{rx} would lose the Plansee-W's property originated from the thermo-mechanical process by recrystallization and SPS-W_r would get thermo-mechanically treated-like property by deformation.

In the OM images of the indented area of the Plansee-W_{rx} (Figure 44 (a) and (b)), cracks formed by indentation were observed though the crack propagation tendency was different. In the OM images of the indented area of the SPS-W_r (Figure 44 (c) and (d)), crack was not found. These results indicate that some amount of deformation might be required to increase the ductility of the tungsten materials.

The hardness of the Plansee-W_{rx} was 310HV30 with STDEV of 2HV. Through the reduction of 10~20% on SPS-W, the hardness values of SPS-W increased. For the 10% reduced SPS-W_2, the hardness was 382HV30 with STDEV of 3HV. In the case of SPS-W_3, the hardness of 10% reduced sample was 370HV30 with STDEV of 4HV and the hardness of 20% reduced samples was 433HV30 with STDEV of 3HV. It was confirmed that the ITER specification hardness (410HV30) could be satisfied by reducing the SPS-W.

AES was utilized to find the reason for the cracking of as-sintered SPS-W and Plansee-W_{rx}. AES is an effective method to observe surface elements of a sample. SPS-W and Plansee-W_{rx} samples were in-situ fractured in AES chamber and the fractured surfaces were observed (Figure 45). In both samples, typical intergranular fractured surfaces could be observed, and impurities such

as S, P, and O were detected on the intergranular fractured surface (Figure 46 and Figure 47). Especially, K was observed in some area of SPS-W_2. Figure 46 and Figure 47 show that SPS-W_2 had higher oxygen contents than Plansee-W_{rx}, and Plansee-W_{rx} had higher phosphorus contents than SPS-W_2. Figure 48 and Figure 49 show the depth profiling results of SPS-W_2 and Plansee-W_{rx} respectively. It can be seen that impurity contents disappeared after sputtering the surface of the sample. As the initially observed surface was intergranular fractured surface, the existence of impurities in grain boundaries were confirmed in both high-density sintered tungsten samples and Plansee-W_{rx}. These results suggest that the impurity contents at the grain boundaries may cause of the intergranular cracking, weaken the bonding between each grain.

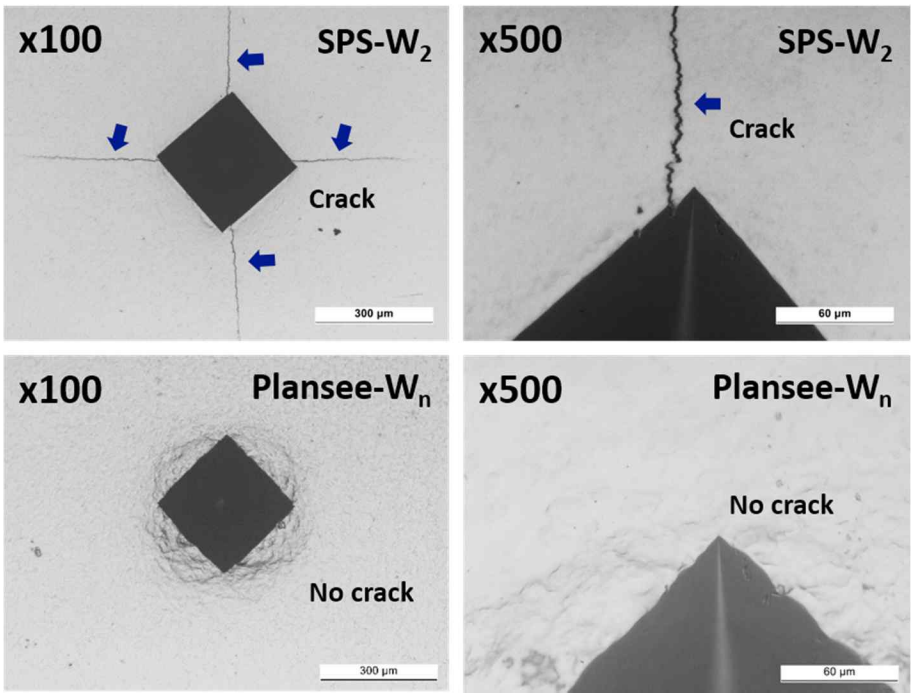

Figure 42. Indented area of SPS-W_2 and Plansee-W_n.

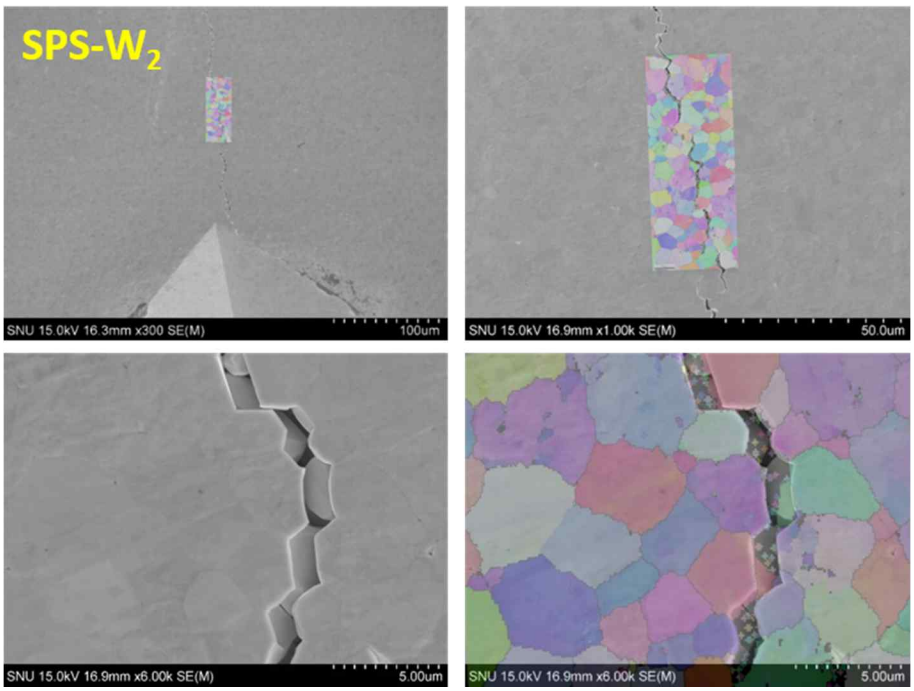

Figure 43. Intergranular cracking behavior of high-density sintered tungsten sample (SPS-W_2).

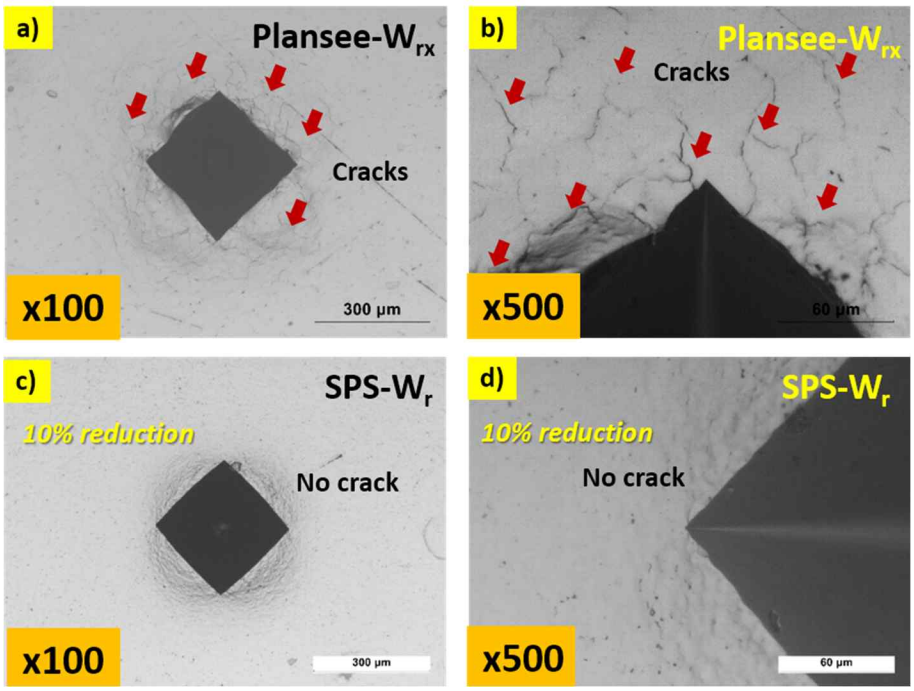

Figure 44. Indented areas of the Plansee-W_{rx} and SPS-W_r.

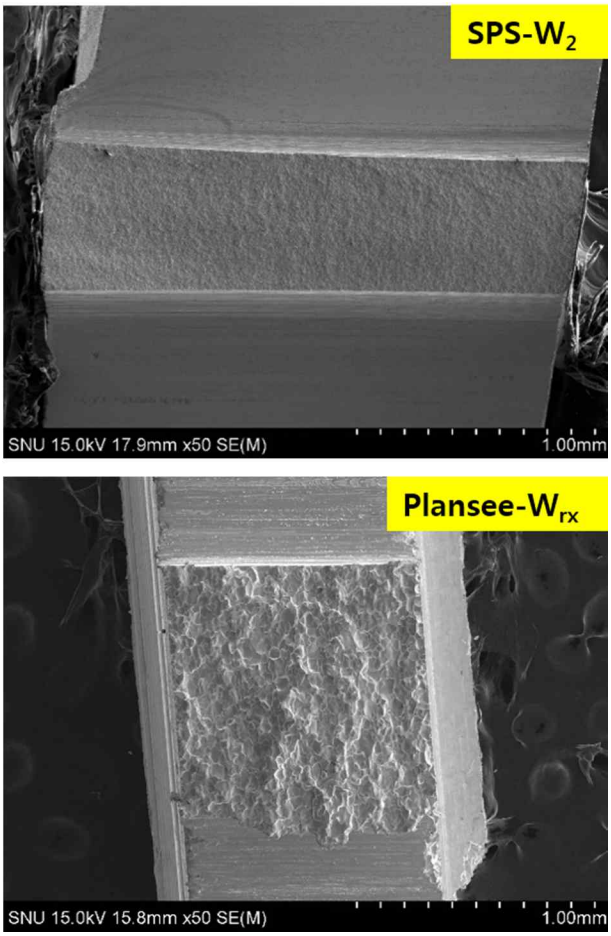

Figure 45. In-chamber fractured surfaces of SPS-W_2 and Plansee-W_{rx}.

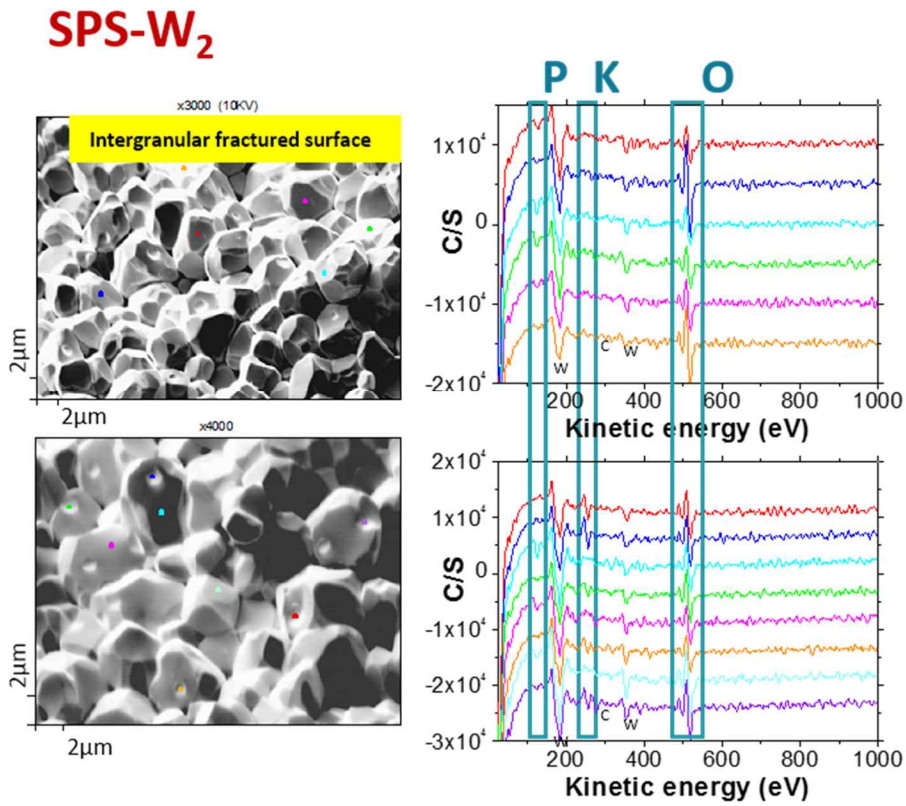

Figure 46. AES point scanning results of SPS-W_2.

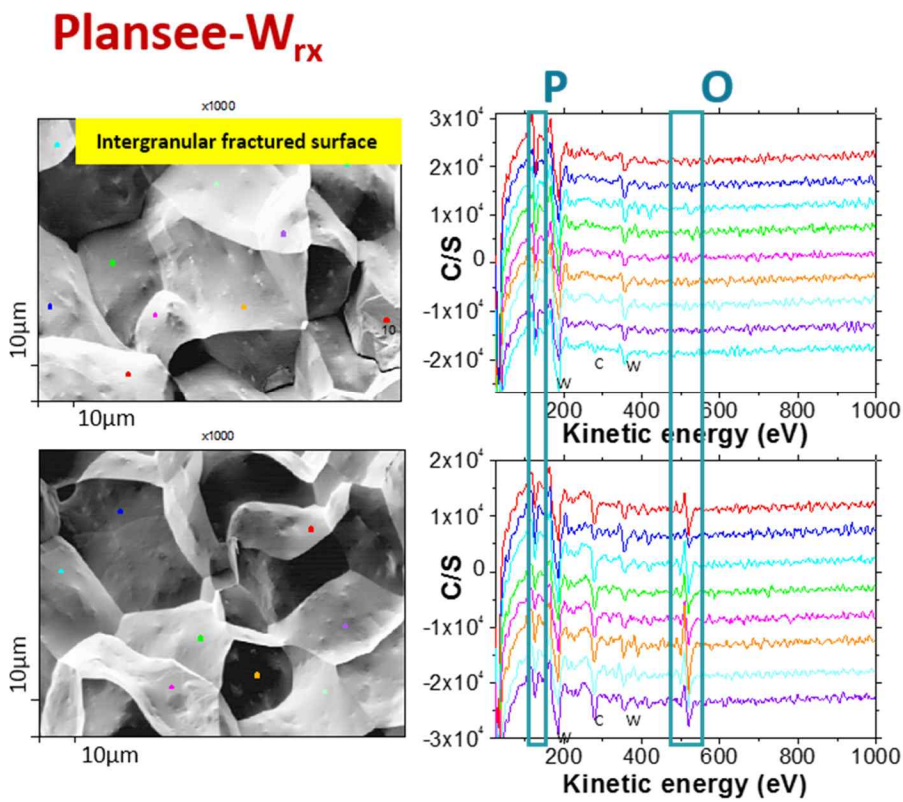

Figure 47. AES point scanning results of Plansee-W$_{rx}$.

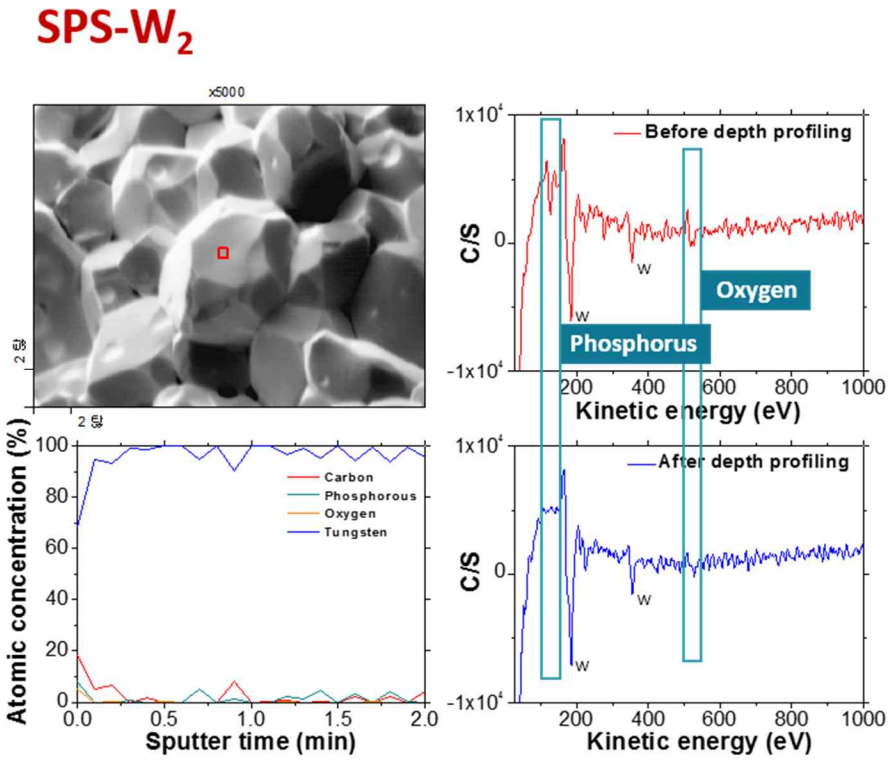

Figure 48. AES depth profiling results of SPS-W_2.

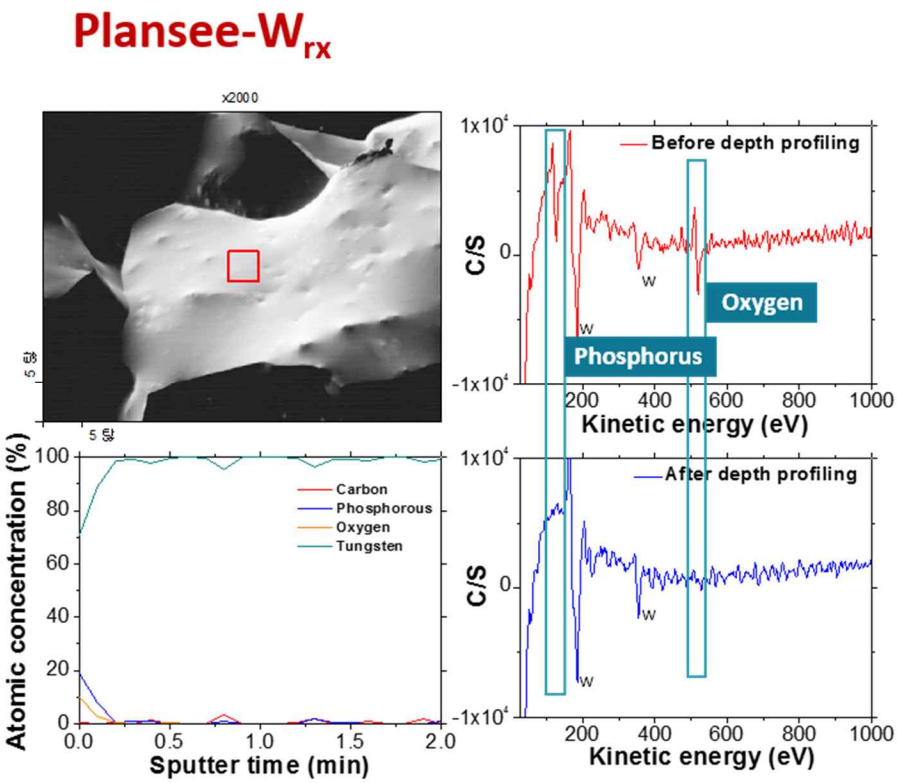

Figure 49. AES depth profiling results of Plansee-W$_{rx}$.

5. Conclusions

In this study, sintering conditions for high-density sintered tungsten samples were obtained using SPS and their thermal stabilities were evaluated. To fabricate high-density sintered tungsten samples, the effects of sintering factors on sintered samples were investigated. The microstructure and properties of sintered samples were feedbacked for the optimization of the sintering conditions and two sintering conditions to obtain high-density sintered tungsten samples with relative density of 99.9% were successfully obtained. The fabricated tungsten samples were HHF tested to evaluate their thermal stability. Comparing with Plansee-W, high-density sintered tungsten samples were confirmed to have more stable microstructure and mechanical property at elevated temperatures. Especially, at 1400°C, which can be considered close to the operation condition of fusion reactor, high-density sintered tungsten samples exhibit better thermal stability comparing to the Plansee-W, showing less changes in microstructure and hardness. Additionally, improvement of mechanical property of high-density sintered tungsten samples was studied. As the high-density sintered tungsten samples were cracked and Plansee-W did not crack after the indentation test, the effect of thermo-mechanical process was investigate. By comparing the cracking behavior of as-sintered and SPS-W_r, Plansee-W and Plansee-W_{rx} after indentation, it was confirmed that some amount of deformation could increase the ductility of tungsten materials with

increasing hardness. Also, the cracks observed in the high-density sintered tungsten samples were revealed to be the intergranular cracking. AES results suggest that the impurity contents on grain boundaries might be the reason for the intergranular cracking of the as-sintered high-density sintered samples and Plansee-W_{rx}.

6. References

[1] G. Pintsuk, Tungsten as a Plasma-Facing Material, Reference Module in Materials Science and Materials Engineering, Volume 4, Pages 551–581 (2012)

[2] A. Miyahara, T. Tanabe, Graphite as plasma facing material, J. Nucl. Mater. 155-157 (1988) 49–57

[3] K. Tokunaga, N. Yoshida, N. Noda, Y. Kubota, S. Inagaki, R. Sakamoto, et al., Behavior of plasma-sprayed tungsten coatings on CFC and graphite under high heat load, J. Nucl. Mater. 266 (1999) 1224–1229

[4] G.S. Cho, K.H. Choe, Characterization of plasma-sprayed tungsten coating on graphite with intermediate layers, Surf. Coat. Technol. 209 (2012) 131–136

[5] You Jung Lee, Hyun-Min Sung, Younggil Jin, Keunho Lee, Chong Rae Park, Gon-Ho Kim, Heung Nam Han, Improvement of mechanical property of air plasma sprayed tungsten film using pulsed electric current treatment, Int. Journal of Refractory Metals and Hard Materials 60 (2016) 99–103

[6] I. Smid, M. Akiba, G. Vieider, L. Plöchl, Development of tungsten armor and bonding to copper for plasma-interactive components, J. Nucl. Mater. 258-263 (1998) 160–172

[7] J. Davis, V. Barabash, A. Makhankov, L. Plöchl, K. Slattery, Assessment of tungsten for use in the ITER plasma facing components, J. Nucl. Mater. 258-263 (1998) 308–312

[8] Y. Ueda, K. Tobita, Y. Katoh, PSI issues at plasma facing surfaces of

blankets in fusion reactors, J. Nucl. Mater. 313-316 (2003) 32–41

[9] S. Wurster, N. Baluc, M. Battabyal, T. Crosby, J. Du, C. García-Rosales, et al., Recent progress in R&D on tungsten alloys for divertor structural and plasma facing materials, J. Nucl.Mater. 442 (2013) 181–189

[10] V. Philipps, Tungsten as material for plasma-facing components in fusion devices, J. Nucl. Mater. 415 (2011) 2–9

[11] T. Weber, J. Aktaa, Numerical assessment of functionally graded tungsten/steel joints for divertor applications, Fusion Eng. Des. 86 (2011) 220–226

[12] R. Orrù, R. Licheri, A.M. Locci, A. Cincotti, G. Cao, Consolidation/synthesis of materials by electric current activated/assisted sintering, Mater. Sci. Eng. R Reports. 63 (2009) 127–287.

[13] N. Saheb, Z. Iqbal, A. Khalil, A.S. Hakeem, N. Al Aqeeli, T. Laoui, et al., Spark plasma sintering of metals and metal matrix nanocomposites: A review, J. Nanomater. 2012 (2012).

[14] http://www.iter.org

[15] J. Roth, E. Tsitrone, T. Loarer, V. Philipps, S. Brezinsek, A. Loarte, et al., Tritium inventory in ITER plasma-facing materials and tritium removal procedures, Plasma Phys. Control. Fusion. 50 (2008)

[16] G.S. Lee, M. Kwon, C.J. Doh, G. Hong, B, K. K, M.H. Cho, et al., Design and construction of the KSTAR tokamak, Nucl. Fusion. 41 (2001) 1515–1523.

[17] http://www.rcp.ijs.si/mic/our_work/applications/fusion/fusion.php

[18] http://iter.rma.ac.be/en/Documents/Pictures

[19] https://www.euro-fusion.org

[20] H.Y. Xu, Y.B. Zhang, Y. Yuan, B.Q. Fu, A. Godfrey, G. De Temmerman, et al., Observations of orientation dependence of surface morphology in tungsten implanted by low energy and high flux D plasma, 443 (2013) 452–457.

[21] M.Y. Ye, H. Kanehara, S. Fukuta, N. Ohno, S. Takamura, Blister formation on tungsten surface under low energy and high flux hydrogen plasma irradiation in NAGDIS-I, J. Nucl. Mater. 313-316 (2003) 72–76.

[22] W. Wang, J. Roth, S. Lindig, C.H. Wu, Blister formation of tungsten due to ion bombardment, J. Nucl. Mater. 299 (2001) 124–131.

[23] S. Kajita, N. Yoshida, R. Yoshihara, N. Ohno, M. Yamagiwa, TEM observation of the growth process of helium nanobubbles on tungsten: Nanostructure formation mechanism, J. Nucl. Mater. 418 (2011) 152–158.

[24] Q. Yang, Y.-W. You, L. Liu, H. Fan, W. Ni, D. Liu, et al., Nanostructured fuzz growth on tungsten under low-energy and high-flux He irradiation, Sci. Rep. 5 (2015) 10959.

[25] G. Federici, C. Skinner, J. Brooks, J. Coad, C. Grisolia, A. Haasz, et al., Plasma-material interactions in current tokamaks and their implications for next step fusion reactors, Nucl. Fusion. 41 (2001) 1967–2137.

[26] Al-Ajlony, J.K. Tripathi, a. Hassanein, Role of carbon impurities on the surface morphology evolution of tungsten under high dose helium ion

irradiation, J. Nucl. Mater. 466 (2015) 569–575.

[27] R.F. Post, Impurity radiation losses from a high temperature plasma, J. Nucl. Energy. Part C, Plasma Physics, Accel. Thermonucl. Res. 3 (2002) 273–286.

[28] S.H. Hong, E.N. Bang, S.T. Lim, J.Y. Lee, S.J. Yang, a. Litnovsky, et al., Preliminary test results on tungsten tile with castellation structures in KSTAR, Fusion Eng. Des. 89 (2014) 1704–1708.

[29] Machlin ES (1959) Applied voltage and the plastic properties of “brittle” rock salt. J Appl Phys 30(7):1109–1110

[30] Z.S. Xu, Z.H. Lai, Y.X. Chen, Effect of current on the recrystallization behavior of cold worked α-Ti, Scr. Metall. 22 (1988) 187–190.

[31] H. Conrad, Thermally activated plastic flow of metals and ceramics with an electric field or current, Mater. Sci. Eng. A 322 (2002) 100–107.

[32] H. Conrad, W.D. Cao, X.P. Lu, A.F. Sprecher, Effect of an electric field on the superplasticity of 7475 Al, Scr. Metall. 23 (1989) 697–702.

[33] X.-P. Lu,W.-D. Cao, A.F. Sprecher, H. Conrad, Influence of an external electric field on the microstructure of superplastically deformed 7475 Al, J. Mater. Sci. 27 (1992) 2243–2250.

[34] C. Li, S. Jiang, K. Zhang, Pulse current-assisted hot-forming of light metal alloy, Int. J. Adv. Manuf. Technol. 63 (2012) 931–938.

[35] J.J. Jones, L. Mears, Thermal response modeling of sheet metals in uniaxial tension during electrically-assisted forming, J. Manuf. Sci. Eng. 135 (2013) 1–

11.

[36] M.J. Kim, K. Lee, K.H. Oh, I.S. Choi, H.H. Yu, S.T. Hong, et al., Electric current-induced annealing during uniaxial tension of aluminum alloy, Scr. Mater. 75 (2014) 58–61.

[37] https://www.plansee.com/en/materials/tungsten.html#c956

[38] H.S. Kim, S.T. Lim, Y. Jin, J.Y. Lee, J.M. Song, G.H. Kim, Recrystallization of bulk and plasma-coated tungsten with accumulated thermal energy relevant to Type-I ELM in ITER H-mode operation, J. Nucl. Mater. 463 (2015) 215–218.

[39] T. Hirai, F. Escourbiac, V. Barabash, A. Durocher, A. Fedosov, L. Ferrand, et al., Status of technology R & D for the ITER tungsten divertor monoblock, J. Nucl. Mater. 463 (2015) 1248–1251.

[40] T. Loewenhoff, S. Bardin, H. Greuner, J. Linke, H. Maier, T.W. Morgan, et al., Impact of combined transient plasma/heat loads on tungsten performance below and above recrystallization temperature, Nucl. Fusion. 55 (2015)

[41] P. Sachenko, J.H. Schneibel, W. Zhang, Effect of Faceting on the Thermal Grain-Boundary Grooving of Tungsten, Philos. Mag. A. 82 (2002)

[42] I.-W. Chen, X.-H. Wang, Sintering dense nanocrystalline ceramics without final-stage grain growth, Nature. 404 (2000) 168–171.

국문초록

본 연구에서는 스파크 플라즈마 소결법을 이용하여 고밀도 순수 텅스텐 소결체 제조 기술을 개발하고, 소결 시편들의 열적 안정성을 평가하였다. 고밀도 텅스텐 소결체 제조 조건 확립을 위해 소결 온도, 시간, 공정, 분말 조건 등 소결 인자의 영향을 도출하였으며, 제조된 소결체들은 미세조직과 물성 분석을 통해 피드백되었다. 이를 통해 고밀도 텅스텐 소결체 제조 조건이 성공적으로 도출되었다. 고밀도 텅스텐 소결체는 고열속 열부하 조건에서 Plansee 사의 상용 ITER 급 텅스텐 소재와 열적 안정성이 비교 분석되었으며, 그 결과 본 연구를 통해 제조 된 고밀도 텅스텐 소결체가 Plansee사의 ITER급 텅스텐 소재보다 고온에서 더 안정적인 미세조직과 기계적 물성을 갖는 것이 확인되었다. 추가적으로, 텅스텐 소재의 대한 기계적 물성 개선에 대한 연구도 진행되었다.

주요어: 플라즈마 대면소재, 텅스텐, 스파크 플라즈마 소결법, 고열속 열부하 시험, 열적 안정성, 전자후방산란, 기계적 물성.

학번 : 2015-20830